SIAM J. Applied Dynamical Systems
Vol. 16, No. 3, pp. 1748–1795

High-Order Parameterization of Stable/Unstable Manifolds for Long Periodic Orbits of Maps*

J. L. Gonzalez† and J. D. Mireles James†

Abstract. This paper develops seminumerical methods for computing high-order polynomial approximations of stable/unstable manifolds attached to long periodic orbits in discrete time dynamical systems. Our approach extends a standard multiple shooting scheme for periodic orbits, allowing us to compute invariant manifolds for periodic orbits without considering compositions of the map. This leads to a system of conjugacy equations characterizing the complete collection of chart maps, with one chart attaching a local stable/unstable manifold to each point along the periodic orbit. We develop a formal series solution for the system of conjugacy equations and show that the coefficients of the series are determined by recursively solving certain linear systems of equations. We derive the recursive equations for a number of example problems in dimensions two and three, with both polynomial and transcendental nonlinearities, and present some numerical results which illustrate the utility of the method. We also highlight some technical issues such as controlling the decay rate of the coefficients and managing truncation errors via a posteriori indicators.

Key words. parameterization method, periodic orbits of maps, multiple shooting, stable and unstable manifolds

AMS subject classifications. 37, 37D, 37M

DOI. 10.1137/16M1090041

1. Introduction.

In this work we compute high-order polynomial approximations of local stable/unstable manifolds attached to periodic orbits in discrete time dynamical systems. Our approach is based on the parameterization method of [12, 13, 14], which is a general functional analytic framework for studying invariant manifolds. The main idea of the parameterization method is to look for chart maps which satisfy certain invariance equations. In the case of stable/unstable manifolds, this invariance equation conjugates the nonlinear dynamics near the fixed point to a simple polynomial model. (In fact, often we can arrange for the polynomial to be linear, see (4) and also Remark 2.6). The parameterization method recovers the dynamics on the invariant manifold in addition to the embedding, and moreover, the chart is not required to be the graph of a function—hence it is possible to follow folds in the embedding. The invariance equation also provides a convenient notion of defect, which is exploited for a posteriori error analysis. The main goal of the present work is to develop a parameterization method optimized for periodic problems and to demonstrate that this method leads to efficient numerical implementations.

*Received by the editors August 19, 2016; accepted for publication (in revised form) by J. van den Berg May 15, 2017; published electronically September 28, 2017.
http://www.siam.org/journals/siads/16-3/M109004.html
Funding: This research was partially supported by NSF grant DMS 1318172.
†Department of Mathematical Sciences, Florida Atlantic University, Boca Raton, FL 33431 (jorgegonzale2013@fau.edu, jmirelesjames@fau.edu).

A period-N orbit for a map $f\colon \mathbb{R}^M \to \mathbb{R}^M$ is a fixed point of the map f^N (f is composed with itself N times), and in principle one could compute invariant manifolds for period-N points by applying the parameterization method to the map f^N. In practice, however, the complexity of the composition f^N grows exponentially in N. The novelty of the present work is a *composition-free* parameterization method for invariant manifolds attached to periodic points. The idea is to extend the usual multiple shooting scheme for the periodic orbit itself to the invariance equation describing the manifold.

More precisely if $p_1, \ldots, p_N \in \mathbb{R}^M$ is a periodic orbit with $m \leq M$ stable (or unstable) eigenvalues, then our method simultaneously finds the Taylor approximations of some functions $P_1, \ldots, P_N\colon \mathbb{R}^m \to \mathbb{R}^M$ where P_j parameterizes a local stable (or unstable) manifold attached to p_j for each $1 \leq j \leq N$. The Taylor approximation is computed numerically to any desired order. Just as in a multiple shooting scheme for the periodic orbit itself, our system of invariance equations involves no compositions, and hence the nonlinearity determining the stable/unstable manifold for the periodic orbit is only as complicated as the original nonlinearity of the model (see (15)).

To illustrate the utility of the method, we implement it for several application problems in dimensions two and three. We discuss a number of computations for one- and two-dimensional manifolds associated with periodic orbits of periods up to 100 for a planar and spatial Hénon-type map. We also show that application of the method is not limited to polynomial maps by computing stable/unstable manifolds for some periodic orbits of the "standard map," which is a system having a trigonometric nonlinearity.

Remark 1.1 (periodic orbits and their stable/unstable manifolds in applied dynamical systems theory). Periodic orbits are fundamental objects of interest in the qualitative theory of dynamical systems. For example, hyperbolic periodic orbits are dense in chaotic sets such as topological horseshoes and many strange attractors [71, 73]. Studying the set of points in which the stable/unstable manifolds intersect leads to bounds on topological entropy and a better understanding of mixing in the system [6, 32]. In these arguments, the more periodic orbits one includes the better the entropy bounds obtained [18, 19]. We can study the way that orbits approach an attractor by considering the local stable manifolds of a large enough collection of periodic points [77]. The attractor itself is well approximated by the unstable manifolds of such a collection.

The implications of Remark 1.1 are illustrated in Figure 1, where we see the stable manifolds (in red) and unstable manifolds (in blue) of a collection of points with periods ranging from 2 to 16 near the Hénon attractor. Points in phase space approach the attractor along the red curves, while the blue curves describe well the structure of the attractor. (See Remark 1.2 below for more details.)

The interested reader could compare the results shown in Figure 1 to similar results discussed in [66, 78]. In particular, see the bottom right frame of Figure 7 in the former reference and the bottom right frame of Figure 4 in the latter. These figures illustrate the results of backward iterating (11 iterates) a local parameterization of the stable manifold of a fixed point (period one orbit) of the Hénon map. Our Figure 1 provides a much more dense view of the hyperbolic structure but involves no iteration of the map; i.e., no continuation methods have been applied to the local parameterizations. This highlights the value of

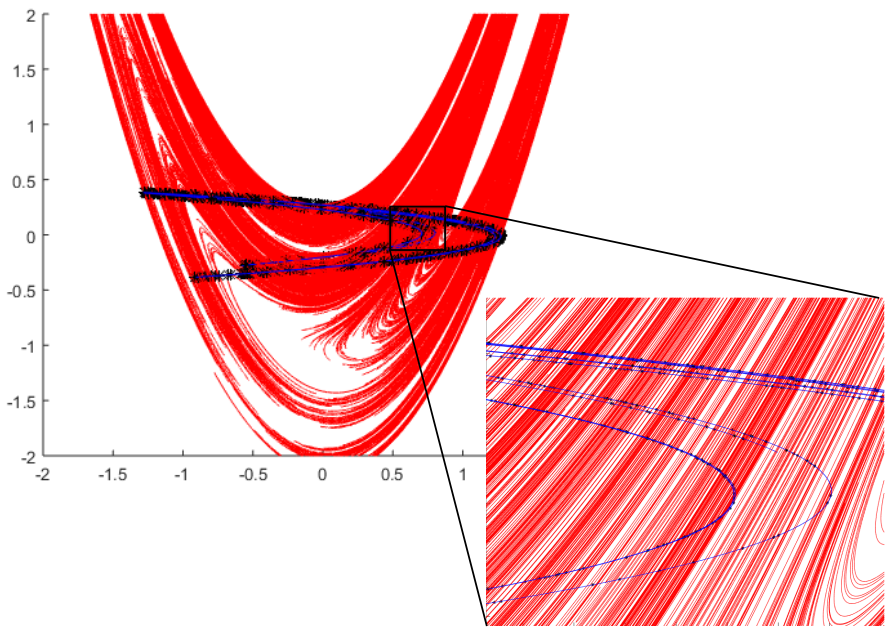

Figure 1. *Periodic orbits and their attached invariant manifolds for the Hénon map. The figure illustrates the parameterized local unstable/stable manifolds for a collection of orbits having period between* 2 and 16. *The periodic orbits are black, unstable manifolds are blue, and stable manifolds are red. Orbits approach the Hénon attractor along the (red) stable manifolds. The unstable manifolds (blue) outline the attractor itself. The picture makes it clear that the stable/unstable manifolds intersect many times, giving rise to heteroclinic/homoclinic tangles. The picture is generated by evaluating a collection of polynomial parameterizations for the local stable/unstable manifolds of the periodic orbits, which does not involve any iteration of the map/continuation algorithms. Computations for the Hénon map are discussed in more detail in section* 4.3.

the parameterization method developed in the present work but also suggests what could be achieved in future studies by combining our local methods with globalization techniques such as those of [66, 78].

We must stress again that the idea of using multiple shooting schemes to study periodic dynamics is standard, having been used to great effect by a number of authors. See, for example, the study of [75] on computer-assisted analysis of stability regions for the quadratic map, the studies of [6, 32] on computer-assisted existence proofs for periodic orbits of maps (the former reference even studies infinite-dimensional discrete time systems), and the more theoretical study of [28]. The present work extends standard multiple shooting analysis to the problem of computing local stable/unstable manifolds.

Remark 1.2 (illustration of results). Figures 1 and 2 illustrate some results obtained using the methods of the present work. Figure 1 shows parameterized local stable/unstable manifolds attached to a collection of periodic orbits for the Hénon map at the classical parameter values. More precisely, the collection contains 1 period two, 1 period four, 2 period six, 4 period seven, 7 period eight, 6 period nine, 10 period ten, 14 period eleven, 13 period twelve, 23 period thirteen, 9 period fourteen, 21 period fifteen, and 14 period sixteen orbits. Each

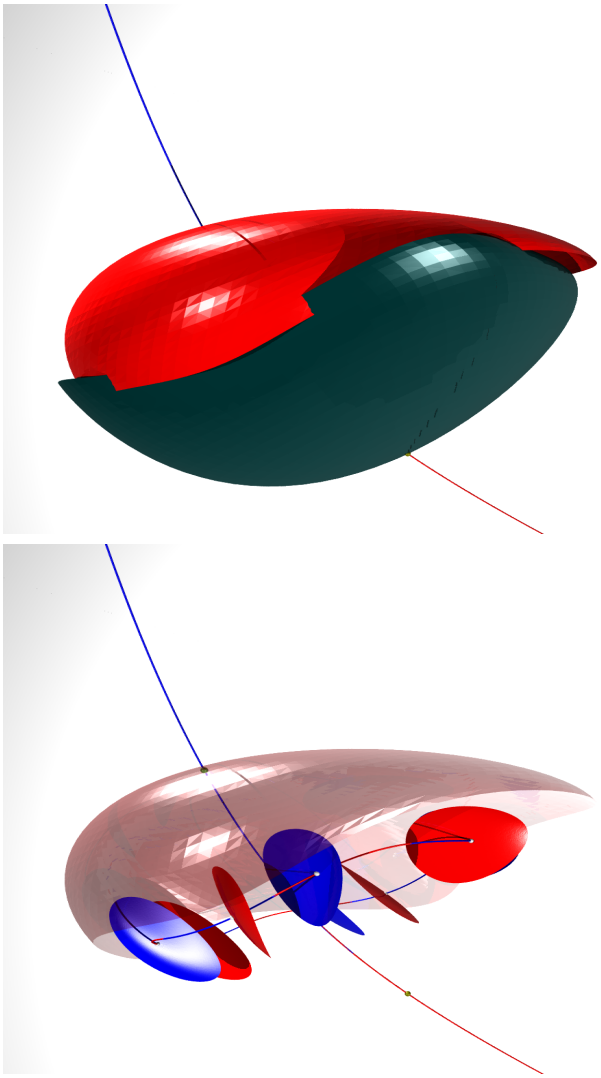

Figure 2. *Vortex bubble and period four subbubble in the Lomelí map: Top: two-dimensional unstable (blue) and two-dimensional stable (red) manifolds attached to the fixed points of the Lomelí map. One-dimensional manifolds are also shown. The two-dimensional manifolds form a "bubble" which encloses all the invariant dynamics of the system. Bottom: dynamics inside the bubble. We locate a pair of period four saddles. The stable/unstable manifolds of the period four orbits form "subbubbles." We compute polynomial parameterization of the one- and two-dimensional manifolds for the period four points using the techniques of the present work. Again, no continuation scheme has been applied to the local parameterizations illustrated in this figure. These computations are discussed further in section 4.5.*

manifold is approximated to Taylor order 25, and the decay rate of the Taylor coefficients is controlled adaptively to ensure that the last coefficients in this expansion are small. A posteriori error bounds for each manifold are below 10^{-14}.

Figure 2 shows results from a similar computation involving two fixed points and two period four orbits of the three-dimensional Lomelí map. This map preserves volume, and

hence there are no attractors. Deliberate computations of hyperbolic structures, such as the ones developed in the present work, facilitate better understanding of the orbit structure of such systems. The manifolds are approximated to Taylor order 25, and the a posteriori error is small. More details for these and other computations are found in section 4.

The curves and surfaces shown in the figures are obtained by evaluating polynomial approximations of the local invariant manifolds. The polynomials are computed using the methods developed in section 3 and implemented as discussed in section 4. The computations illustrated in the figures, and discussed throughout the present work, make no use of numerical continuation or globalization methods for the local manifolds. This is not to say that local parameterizations should never be globalized. Rather, the present work focuses on results which can be achieved priori to continuation/globalization. We leave to a future study the task of continuing our results.

We make an effort to work out quite explicitly the derivation of the recursion relations defining the Taylor series coefficients of our polynomial approximations, as it is hoped that the present work constitutes a stand-alone exposition in this sense. Nevertheless these formal series arguments can be automated using software packages such as those discussed in [45, 59]. Development of general-purpose software, however, is beyond the scope of the present study.

Remark 1.3 (a posteriori analysis and validated numerics). As already mentioned above, one of the strengths of the parameterization method is that it provides a notion of a posteriori error (or defect). In other words, since the desired parameterizations solve an operator equation, we can always plug our approximate solution into the equation, and asses (via some convenient choice of norm) how close the result is to zero. In the present work we use the a posteriori error as an indicator of the quality of our computations.

Of course small defects do not imply small truncation errors, and it is desirable to have a more refined a posteriori analysis. Indeed, via a blend of pen- and- paper analysis with deliberate control of round-off errors, it is possible to obtain mathematically rigorous computer-assisted error bounds associated with the polynomial approximations. Several works in this vein, for both finite- and infinite-dimensional dynamical systems, are [10, 43, 44, 63, 65, 76]. Developing validated numerics for the parameterization method of the present work is the topic of an upcoming study by the authors.

2. Background.

This section reviews some basic notions from the qualitative theory of dynamical systems and provides a brief review of the parameterization method for stable/unstable manifolds of fixed points. The reader familiar with the parameterization method may want to skip ahead to section 3 and refer back to this section only as needed. The reader wishing to review the parameterization method may want to skim section 2.2.

Let $x = (x_1, \dots, x_M) \in \mathbb{R}^M$ denote a point in Euclidean M-space, and endow $\mathbb{R}^M$ with the norm

$$\|x\| := \max_{1 \le j \le M} |x_j|,$$

where $|\cdot|$ denotes the usual absolute value. Let

$$B_r^M(x) := \{y \in \mathbb{R}^M : \|x - y\| < r\}$$

denote the ball (actually, cube) of radius r about x in this norm. If $E \subset \mathbb{R}^M$ is compact and $x \in \mathbb{R}^M$, define

$$d(x, E) := \inf_{y \in E} \|x - y\|,$$

the distance from x to E.

When discussing power series, we employ the following notation. If $P\colon \mathbb{R}^m \to \mathbb{R}^M$ is analytic at $p_0 \in \mathbb{R}^M$, then P has a power series representation

$$P(\theta) = \sum_{|\alpha|=0}^{\infty} p_\alpha \theta^\alpha = \sum_{\alpha_1=0}^{\infty} \cdots \sum_{\alpha_m=0}^{\infty} p_{\alpha_1,\ldots,\alpha_m} \theta_1^{\alpha_1} \cdots \theta_m^{\alpha_m},$$

where $\alpha = (\alpha_1, \ldots, \alpha_m) \in \mathbb{N}^m$ is an m-dimensional multi-index,

$$|\alpha| := \alpha_1 + \cdots + \alpha_m,$$

$p_\alpha \in \mathbb{R}^M$ for each α, and

$$\theta^\alpha := \theta_1^{\alpha_1} \cdots \theta_m^{\alpha_m}.$$

2.1. Stable/unstable manifold for discrete time dynamical systems. Consider a diffeomorphism $f : \mathbb{R}^M \to \mathbb{R}^M$ with fixed point p. (All of the examples considered in the present work are in fact analytic maps with analytic inverse.) Suppose that p is a hyperbolic fixed point of f, i.e., that no eigenvalues of $Df(p)$ lie on the unit circle. Then there are $m_s, m_u \in \mathbb{N}$ with $m_s + m_u = M$, so that $Df(p)$ has m_s stable eigenvalues and m_u unstable eigenvalues (counted with multiplicity). We then label the eigenvalues as $\lambda_1^s, \ldots, \lambda_{m_s}^s, \lambda_1^u, \ldots, \lambda_{m_u}^u$ with

$$0 < |\lambda_{m_s}^s| \leq \cdots |\lambda_1^s| < 1 < |\lambda_1^u| \leq \cdots |\lambda_{m_u}^u|.$$

Let $\xi_1^u, \ldots, \xi_{m_u}^u, \xi_1^s, \ldots, \xi_{m_s}^s \in \mathbb{R}^M$ denote a choice of linearly independent (possibly generalized) eigenvectors.

Let $U \subset \mathbb{R}^M$ be an open neighborhood of p. The local stable set of p relative to U is

$$W_{\text{loc}}^s(p, U) := \left\{ x \in \mathbb{R}^M : f^n(x) \in U \text{ for all } n \geq 0 \right\}.$$

By the stable manifold theorem (see, for example, [67] for discussion and proof) there exists an open neighborhood $V \subset \mathbb{R}^M$ of p so that

(i) the local stable set $W_{\text{loc}}^s(p, V)$ is a smooth, embedded, m_s-dimensional disk. If f is analytic then the embedding is analytic.

(ii) $W_{\text{loc}}^s(p, V)$ is tangent to the stable eigenspace of $Df(p)$ at p; i.e., the vectors $\xi_1^s, \ldots, \xi_{m_s}^s$ span the tangent space of $W_{\text{loc}}^s(p, V)$ at p.

(iii) if $x \in W_{\text{loc}}^s(p, V)$, then

$$\lim_{n \to \infty} f^n(x) = p.$$

We refer to any local stable set $W^s_{\text{loc}}(p, V)$ satisfying (i)–(iii) above as a local stable manifold for p. We say that $W^s_{\text{loc}}(p)$ is a local stable manifold at p if $W^s_{\text{loc}}(p) = W^s_{\text{loc}}(p, V)$ satisfies (i)–(iii) above with V some open neighborhood of p. Note that if $W^s_{\text{loc}}(p, V)$ has (i)–(iii) above and $B^M_r(p) \subset V$, then $W^s_{\text{loc}}(p, B^M_r(p))$ has (i)–(iii) as well; i.e., local stable manifolds are not unique.

Since f is invertible given any local stable manifold $W^s_{\text{loc}}(p, V)$, we can define the set

$$W^s(p) = \bigcup_{n=0}^{\infty} f^{-n}\left[W^s_{\text{loc}}(p)\right] = \left\{x \in \mathbb{R}^M \mid f^n(x) \to p \text{ as } n \to \infty\right\}. \tag{1}$$

The resulting set $W^s(p)$ is a globally invariant manifold (which may not be an embedded disk). We refer to $W^s(p)$ as *the* stable manifold of p, as $W^s(p)$ does not depend on the choice of local stable manifold.

With these considerations applied to f^{-1} at p, let us define local unstable manifolds, which we denote by $W^u_{\text{loc}}(p)$ with analogous definition. (We remark that if p is a hyperbolic fixed point of a smooth map f, then f^{-1} exists at least locally, and the assumption above that f is a diffeomorphism on $\mathbb{R}^M$ is not actually needed to define the local unstable manifold. However, this fact is not used in the present work.) The set

$$W^u(p) = \bigcup_{n=0}^{\infty} f^{n}\left[W^u_{\text{loc}}(p)\right] = \left\{x \in \mathbb{R}^M \mid f^{-n}(x) \to p \text{ as } n \to \infty\right\}$$

is a unique globally defined invariant manifold, which we refer to as *the* unstable manifold of p.

Remark 2.1 (linear approximation of the local stable/unstable manifolds). Even when the map $f\colon \mathbb{R}^M \to \mathbb{R}^M$ is explicitly known, closed form expressions for the local stable/unstable manifolds $W^{s,u}_{\text{loc}}(p)$ are rarely available. In applications, we are interested in approximating these manifolds, and part (ii) of the stable manifold theorem provides a first-order approximation. More precisely, suppose that the vectors $\xi^s_1, \ldots, \xi^s_{m_s}$ are all scaled to have length one, and define the $M \times m_s$ matrix as

$$[\xi^s_1 | \cdots | \xi^s_{m_s}] = A_s;$$

i.e., A_s is the matrix with columns given by the (generalized) eigenvectors. Then the parameterization $P^1\colon \mathbb{R}^{m_s} \to \mathbb{R}^M$ given by

$$P^1(\theta) := p + A_s\theta, \qquad \theta := (\theta_1, \ldots, \theta_{m_s})$$

approximates $W^s_{\text{loc}}(p)$ to first order. More precisely, let

$$B^{m_s}_\delta(0) := \{\theta \in \mathbb{R}^{m_s} : \|\theta\| < \delta\}.$$

The restriction of P^1 to $B^{m_s}_\delta(0)$ is a quadratically good approximation of the stable manifold in the sense that

$$\sup_{\theta \in B^{m_s}_\delta(0)} \operatorname{dist}\left(P^1(\theta), W^s_{\text{loc}}(p)\right) \le C\|\theta\|^2,$$

though in practice more work is required to obtain estimates on the magnitude of C. Nevertheless, combining the observation above with (1) leads to various algorithms for approximating $W^s(p)$. This point is discussed in more detail in section 2.4. Similar considerations lead to a linear approximation of the local unstable manifold by the unstable (generalized) eigenvectors.

Remark 2.2. To define the linear approximation P^1 in Remark 2.1, it is necessary to fix a choice of scalings for the (generalized) eigenvectors, and of course this choice is not unique. In general the size of the neighborhood on which the linear approximation gives quadratically good approximation depends on the choice of scalings. For example, in Remark 2.1 we would have obtained exactly the same results by taking the (generalized) eigenvectors to have scalings

$$\|\xi_j^s\| = \delta, \qquad 1 \le j \le m_s,$$

and restricting the domain of P^1 to the unit ball $B_1^{m_s}(0)$.

This nonuniqueness is inherent in many schemes for approximating the stable manifold and plays an important role in what follows. The issue is not surprising, as nonuniqueness appears already in the definition of the local stable manifold (i.e., there is one local stable manifold for every appropriate choice of neighborhood of the fixed point). In the case of the linear approximation, the choice of scalings is more or less arbitrary, and we might as well take unit vectors as in Remark 2.1. However, when we study power series methods, we will see that the freedom to choose the (generalized) eigenvector scalings provides control over the decay rates of the Taylor coefficients. It turns out that manipulating these decay rates is then useful for stabilizing numerical computations.

2.2. Review of the parameterization method. Suppose that f, p, and m_s are as in section 2.1. Throughout the remainder of this section we assume that $m = m_s > 0$ and let $\lambda_1, \ldots, \lambda_m$, and $\xi_1, \ldots, \xi_m$ denote, respectively, the stable eigenvalues and an associated choice of linearly independent (generalized) eigenvectors. Again, by the stable manifold theorem there is a local stable manifold $W^s_{\mathrm{loc}}(p)$, which is geometrically a smooth embedded disk tangent to the stable (generalized) eigenspace at $p \in \mathbb{R}^M$. We are interested in smooth injective maps $P\colon B_1^m(0) \to \mathbb{R}^M$ having

$$P(0) = p \qquad \text{and} \qquad \frac{\partial}{\partial \theta_j} P(\theta) = \xi_j \qquad \text{for each } 1 \le j \le m, \tag{2}$$

and

$$P\left[B_1(0)^m\right] \subset W^s(p), \tag{3}$$

i.e., charts for the local stable manifold. Clearly if P is one such chart, then any reparameterization of P is again a chart. Thus, the parameterization P just discussed cannot be unique, and we are free to impose additional constraints.

The idea of the *parameterization method* [12, 13, 14] is to look for a smooth function $P\colon B_1^m(0) \to \mathbb{R}^M$ satisfying not only the first-order constraints of (2), and the conjugacy equation

$$f[P(\theta_1, \ldots, \theta_m)] = P(\lambda_1\theta_1, \ldots, \lambda_m\theta_m) \tag{4}$$

for all $\theta \in B_1^m(0)$. The situation is illustrated in Figure 3. Several useful results for the parameterization method are summarized below. First we need the following definition.

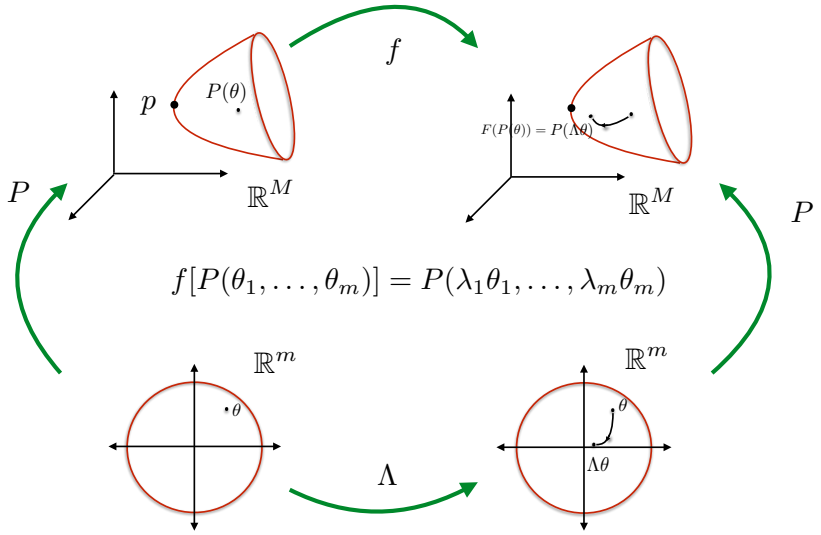

Figure 3. *Cartoon illustrating the conjugacy relation of (4). Here Λ is the diagonal matrix of eigenvalues, and f is the nonlinear map. The goal of the parameterization method is to find a chart P which makes the diagram commute.*

Definition 2.3 (nonresonant eigenvalues). *We say that the stable eigenvalues $\lambda_1, \ldots, \lambda_m$ are nonresonant if*

$$\lambda_1^{\alpha_1} \cdots \lambda_m^{\alpha_m} \neq \lambda_j \quad \text{with } 1 \leq j \leq m$$

for all $\alpha = (\alpha_1, \ldots, \alpha_m) \in \mathbb{N}^m$ with $|\alpha| = \alpha_1 + \cdots + \alpha_m \geq 2$, that is, if no product of positive powers of the stable eigenvalues is again a stable eigenvalue.

First we note that, despite first appearances, Definition 2.3 imposes only a finite number of constraints on the eigenvalues. To see this, let

$$\mu_* = \min_{1 \leq j \leq m} |\lambda_j| \quad \text{and} \quad \mu^* = \max_{1 \leq j \leq m} |\lambda_j|$$

denote, respectively, the smallest and largest moduli of the stable eigenvalues, and note that for any multi-index $\alpha \in \mathbb{N}^m$, we have the bound

$$\begin{aligned} |\lambda_1^{\alpha_1} \cdots \lambda_m^{\alpha_m}| &\leq (\mu^*)^{\alpha_1} \cdots (\mu^*)^{\alpha_m} \\ &= (\mu^*)^{|\alpha|}. \end{aligned}$$

Then a resonance is impossible for any $\alpha \in \mathbb{N}^m$ with

$$(\mu_*)^{|\alpha|} > \mu^*,$$

and we conclude that a necessary condition for a resonance is that

$$2 \leq |\alpha| \leq \frac{\ln(\mu^*)}{\ln(\mu_*)}. \tag{5}$$

Then it is enough to check the resonance conditions only for α as in (5), emphasizing that ruling out a resonance is a finite check.

Definition 2.4 (eigenvector scalings). *Suppose that*

$$\|\xi_1\| = s_1, \ldots, \|\xi_m\| = s_m.$$

We refer to the collection of numbers $s_1, \ldots, s_m > 0$ *as the scalings of the (generalized) eigenvectors and write*

$$s = \max_{1 \le j \le m} (s_j).$$

The following theorem summarizes a number of basic results. Note that from this point forward we impose the additional assumption that the differential is diagonalizable (see, however, Remark 2.6 below). Proofs of these results can be extracted from the much more general discussion in [12]. Under these assumptions the following statements hold

Lemma 2.5. *Let* $f\colon \mathbb{R}^M \to \mathbb{R}^M$ *be an invertible map, and let* $p \in \mathbb{R}^M$ *be a fixed point of* f. *Suppose that* f *is differentiable in a neighborhood of* p, *and assume that the differential* $Df(p)$ *is a diagonalizable matrix. Let* $\lambda_1, \ldots, \lambda_m \in \mathbb{C}$ *denote the stable eigenvalues of* $Df(p)$, *and let* $\xi_1, \ldots, \xi_m \in \mathbb{R}^M$ *denote an associated choice of linearly independent eigenvectors.*

- *If* $P\colon B_1^m(0) \to \mathbb{R}^M$ *is a smooth solution of* (4) *satisfying the first-order constraints given by* (2), *then* P *is a chart map for a local stable manifold of* p.
- *If* $\lambda_1, \ldots, \lambda_m$ *are nonresonant, in the sense of Definition* 2.3, *then there exists an* $\epsilon > 0$ *so that for every choice of eigenvectors with scalings* $s_1, \ldots, s_m$ *as in Definition* 2.4 *having* $s_1, \ldots, s_m \le \epsilon$, (4) *has a solution* $P\colon B_1^m(0) \to \mathbb{R}^M$ *subject to the constraints of* (2). *The solution* P *is unique up to the choice of the eigenvectors.*
- *If* $f \in C^k(\mathbb{R}^M)$, *then* $P \in C^k(B_1^m(0), \mathbb{R}^M)$ *as well.* $k \in \{\infty, \omega\}$ *are included in this claim.*

Now assume that f is analytic near p. Then Lemma 2.5 says that for some choice of eigenvector scalings a parameterization P solving (4) exists, and that the function P is analytic. Then it is natural to look for a power series solution

$$P(\theta) = \sum_{|\alpha|=0}^{\infty} p_\alpha \theta^\alpha.$$

P satisfies the first-order constraints of (2) if we require that

$$p_{\mathbf{0}} = p$$

and

$$p_{e_j} = \xi_j \quad \text{for} \quad 1 \le j \le m_s,$$

where $\mathbf{0} = (0, \ldots, 0) \in \mathbb{N}^{m_s}$ is the m_s-dimensional zeroth-order multi-index and $e_j = (0, \ldots, 1, \ldots, 0)$ are the standard basis vectors for $\mathbb{N}^{m_s}$.

To work out the higher-order coefficients p_α with $|\alpha| \ge 2$, one expands (4) in terms of this power series, matches like powers of θ, and solves the resulting recurrence equations order by order. This computation results in a *homological equation* of the form

$$\left[Df(p) - \lambda_1^{\alpha_1} \cdots \lambda_{m_s}^{\alpha_{m_s}} \mathrm{Id}\right] p_\alpha = S_\alpha, \tag{6}$$

where S_α is a function only of the coefficients p_β with $|\beta| < |\alpha|$, and the form of S_α is completely determined by the nonlinearity of f. Observe that (6) provides a linear equation for the Taylor coefficients of the unknown parameterization.

Observe that as long as the eigenvalues are nonresonant in the sense of Definition 2.3, the homological equation (6) is uniquely solvable, and the parameterization P is formally well defined. Once S_α is known explicitly, numerical algorithms for computing the parameterization P are obtained by solving (6) to the desired order.

The derivation of the homological equations are worked out in detail (and in greater generality) in section 3.1 of [12]. Nevertheless for specific examples it is usually desirable (even necessary) to derive the homological equations from scratch in order to obtain the explicit dependence of S_α on the lower-order terms. In section 2.3 we illustrate such a derivation for the composition of the Hénon map with itself. This computation facilitates comparison of the multiple shooting scheme of the present work with a naive application of the parameterization to the composition map as discussed in section 4.2. Other similar computations are found in [30], in sections 2.2 and 2.3 of [62], and in section 3.1 of [15].

Remark 2.6.

- These developments apply to the unstable manifold with only the obvious changes; i.e., one considers exactly the same conjugacy given in (4) and is led to exactly the same homological equation as given by (6), with the only change being that stable eigenvalues/eigenvectors must be replaced by the unstable eigenvalues/eigenvectors. General treatment of the parameterization method is found in the work of [12, 13, 14]. Several papers focusing on numerical aspects of the parameterization method for stable/unstable manifolds of fixed points for maps are [3, 61, 62, 64, 65]. Many additional extensions and applications of these techniques, as well as a thorough discussion of the literature, are found in the recent book of [39].
- Of course in a particular application it is always possible that a resonance will occur. Indeed, for problems with special symmetries, or problems in which we vary a parameter, resonances are sometimes unavoidable. When there is a resonance it is not possible to analytically conjugate to the linear dynamics, even though the map f is analytic. Yet this is not the end of the story, as the method can still succeed after modifying the conjugacy. In fact, one conjugates to a polynomial rather than a linear map, choosing the polynomial to "kill off" the resonant terms. Similar remarks hold in the nondiagonalizable case, i.e., when we have repeated eigenvalues/generalized eigenvectors. These degenerate cases are worked out in full detail in [12]. The end result is that the parameterization method always applies, once resonances are accounted for. See also the work of [76] for numerical implementation, and a posteriori analysis of the resonant cases. More general nonresonance conditions are studied in [20].

2.3. A first worked out example: Homological equations for a fixed point of the Henon-2 map. The Henon map $f\colon \mathbb{R}^2 \to \mathbb{R}^2$ is the quadratic polynomial diffeomorphism of the plane given by

$$f(x,y) = \begin{pmatrix} 1 + y - ax^2 \\ bx \end{pmatrix}, \tag{7}$$

with $a, b \in \mathbb{R}$. The map is invertible with quadratic inverse. For a much more complete discussion see [41].

In this section we consider the mapping $g\colon \mathbb{R}^2 \to \mathbb{R}^2$ defined by

$$g(x,y) := (f \circ f)(x,y) = \begin{pmatrix} 1 - a + bx - 2ay - ay^2 + 2a^2x^2 + 2a^2yx^2 - a^3x^4 \\ b + by - abx^2 \end{pmatrix}, \tag{8}$$

i.e., one composition of the Henon map with itself. Our interest in this map comes from the fact that if $p_0 \in \mathbb{R}^2$ is fixed for g but not for f, then p_0 is period two for the Hénon map. Moreover the stable/unstable manifolds of the fixed point p_0 for g are the stable/unstable manifolds for the period two orbit in the Hénon map.

In this section we derive, as an exercise, the homological equations associated with g. This exercise serves two purposes; first, to review the classical use of the parameterization as a tool for studying invariant manifolds attached to fixed points; and second, to use the homological equations derived here in section 4.2 to make some comparisons between a naive application of the parameterization method to the composition map and the multiple shooting parameterization method of the present work.

Let $Dg(p_0)$ denote the Jacobian differential of g at p_0, and suppose that $\lambda \in \mathbb{R}$ is a stable (or unstable) eigenvalue of $Dg(p_0)$. Assume that $Dg(p_0)$ is diagonalizable, and let $\xi \in \mathbb{R}^2$ denote an associated eigenvector. We seek

$$P(\theta) = \sum_{n=0}^{\infty} p_n \theta^n = \sum_{n=0}^{\infty} \begin{pmatrix} u_n \\ v_n \end{pmatrix} \theta^n,$$

which satisfies the invariance (4). More precisely, we require that

$$\begin{pmatrix} u_0 \\ v_0 \end{pmatrix} = p_0 \quad \text{and} \quad \begin{pmatrix} u_1 \\ v_1 \end{pmatrix} = \xi,$$

and that P is a solution of

$$g(P(\theta)) = P(\lambda\theta). \tag{9}$$

Expanding both sides of (9) as power series using Cauchy products and matching like powers of θ leads to

$$\begin{pmatrix} bu_n - 2av_n - a\displaystyle\sum_{k=0}^{n} v_{n-k}v_k + 2a\sum_{k=0}^{n} u_{n-k}u_k + 2a^2(v*u*u)_n - a^3(u*u*u*u)_n \\ bv_n - ab\displaystyle\sum_{k=0}^{n} u_{n-k}u_k \end{pmatrix}$$

$$= \lambda^n \begin{pmatrix} u_n \\ v_n \end{pmatrix} \tag{10}$$

for $n \geq 2$, and where (for the sake of brevity) the higher-order Cauchy products are written as

$$(v * u * u)_n := \sum_{k=0}^{n} \sum_{j=0}^{k} v_{n-k} u_{k-j} u_j$$

and

$$(u * u * u * u)_n := \sum_{k=0}^{n} \sum_{j=0}^{k} \sum_{l=0}^{j} u_{n-k} u_{k-j} u_{j-l} u_l.$$

To obtain recurrence relations, we isolate terms of order n, many of which are locked up in the Cauchy products. Thus,

$$\sum_{k=0}^{n} v_{n-k} v_k = 2 v_0 v_n + \sum_{k=1}^{n-1} v_{n-k} v_k$$

and

$$\sum_{k=0}^{n} u_{n-k} u_k = 2 u_0 v_n + \sum_{k=1}^{n-1} u_{n-k} u_k.$$

Similarly,

$$(v * u * u)_n = 2 v_0 u_0 u_n + u_0^2 v_n + \widehat{(v * u * u)}_n$$

and

$$(u * u * u * u)_n = 4 u_0^3 u_n + \widehat{(u * u * u * u)}_n,$$

where

$$\widehat{(v * u * u)}_n := \sum_{k=0}^{n} \sum_{j=0}^{k} \hat{\delta}_{kj}^{nk} v_{n-k} u_{k-j} u_j,$$

$$\widehat{(u * u * u * u)}_n := \sum_{k=0}^{n} \sum_{j=0}^{k} \sum_{l=0}^{j} \hat{\delta}_{kjl}^{nkj} u_{n-k} u_{k-j} u_{j-l} u_l,$$

$$\hat{\delta}_{kj}^{nk} := \begin{cases} 0 & \text{if } k = n \text{ and } j = k, \\ 0 & \text{if } k = n \text{ and } j = 0, \\ 0 & \text{if } k = 0 \text{ and } j = 0, \\ 1 & \text{otherwise} \end{cases}$$

and

$$\hat{\delta}_{kjl}^{nkj} := \begin{cases} 0 & \text{if } k = n,\ j = n,\ \text{and } l = n, \\ 0 & \text{if } k = n,\ j = n,\ \text{and } l = 0, \\ 0 & \text{if } k = n,\ j = 0,\ \text{and } l = 0, \\ 0 & \text{if } k = 0,\ j = 0,\ \text{and } l = 0, \\ 1 & \text{otherwise.} \end{cases}$$

The point is that these "hatted" products are iterated Cauchy products with terms of order n-removed.

We now isolate the terms of order n on the left-hand side and obtain from (10) that

$$\begin{pmatrix} bu_n - 2av_n - 2av_0v_n + 4a^2u_0u_n + 4a^2v_0u_0u_n + 2a^2u_0^2v_n - 4a^3u_0^3u_n \\ bv_n - 2abu_0u_n \end{pmatrix} - \lambda^n \begin{pmatrix} u_n \\ v_n \end{pmatrix} = s_n, \tag{11}$$

where the sum

$$s_n := \begin{pmatrix} a\sum_{k=1}^{n-1} v_{n-k}v_k - 2a^2\sum_{k=1}^{n-1} u_{n-k}u_k - 2a^2\widehat{(v*u*u)}_n + a^3\widehat{(u*u*u*u)}_n \\ ab\sum_{k=1}^{n-1} u_{n-k}u_k \end{pmatrix} \tag{12}$$

has no dependence on u_n, v_n. Moreover, noting that

$$Dg(x,y) = \begin{pmatrix} b + 4a^2x + 4a^2yx - 4a^3x^3 & -2a - 2ay + 2a^2x^2 \\ -2abx & b \end{pmatrix},$$

we see that the left-hand side of (11) becomes

$$\left[\begin{pmatrix} b + 4a^2u_0 + 4a^2v_0u_0 - 4a^3u_0^3 & -2a - 2av_0 + 2a^2u_0^2 \\ -2abu_0 & b \end{pmatrix} - \lambda^n \begin{pmatrix} 1 & 0 \\ 0 & 1 \end{pmatrix}\right] \begin{pmatrix} u_n \\ v_n \end{pmatrix}$$

$$= [Dg(u_0,v_0) - \lambda^n \mathrm{Id}]\, p_n,$$

confirming that the homological have the form claimed in (6) (as they must). More importantly, the calculation provides the explicit form of s_n, which was a priori unknown. Solving the homological equations

$$[Dg(u_0,v_0) - \lambda^n \mathrm{Id}]\, p_n = s_n$$

for $2 \le n \le K$, with s_n as defined in (12), leads to the Kth-order polynomial approximation

$$P^K(\theta) = \sum_{n=0}^{K} p_n \theta^n$$

of the local stable/unstable manifold attached to p_0.

2.4. Related literature: Numerical computation of local stable/unstable manifolds and growing or continuing the global manifold. Two issues have to be considered in any discussion of computational methods for stable/unstable manifolds. First is the local computation near the fixed/periodic orbit, and second is the numerical continuation of the local patch. These two steps have their own distinct flavors, and a growing body of literature is devoted to each.

The simplest approximation of the local stable/unstable manifold is the linear approximation by the eigenspace already mentioned in Remark 2.2. The linear approximation is widely used and is sufficient for many applications. The idea of studying an invariance equation to obtain the jets of an invariant object appears as early as the work of Poincaré (see, for example, the historical discussion in Appendix A of [14]), and numerical methods based on this idea go back to the work of [30]. See also the lecture notes of [70]. Since then, many authors have expanded this research, and a small (and incomplete) sample of works which focus on high-order numerical approximation of stable/unstable manifolds attached to fixed points of maps includes [3, 9, 43, 62]. These works discuss many additional references. The reader interested in these techniques can consult the recent book of [39] for an overview of the literature, many generalizations to quasi-periodic solutions and their invariant sets, and applications to ODEs.

Given a good local approximation of the stable/unstable manifold, one uses continuation techniques such as those discussed in [48, 49] to increase the previously computed local approximation of the manifold. For the case of differential equations, we also mention the method of geodesic level sets [37, 50, 51], the method of boundary value problem continuation of trajectories [52], the method of fat trajectories [40], the PDE formulation of [37], as well as the set oriented methods of [21]. The methods of [21] apply to maps as well. In many applications the continuation/globalization methods just mentioned are seeded with the linear approximation of the stable/unstable manifold by the associated stable/unstable eigenspace. Yet none of the methods just mentioned depends on this; that is, they could instead be seeded with larger local patches of manifold given by some high-order approximation, perhaps providing improved results.

The two studies [35, 79] explore the possibility of building adaptive continuation methods seeded with high-order parameterizations of the local stable/unstable manifolds. In these works the local manifold is computed to any desired order using the parameterization method (much as in the present work), and then a larger portion of the manifold is grown by adaptively iterating a mesh composed of Bézier triangle patches. These works illustrate nicely what can be achieved by combining the parameterization method with sophisticated continuation techniques.

In applications computing stable/unstable manifolds is a first step toward understanding global dynamics of nonlinear systems. We refer, for example, to the numerical studies of global bifurcations and preturbulence for the Lorenz system [1, 27], global consequences of bifurcations at infinity such as α-flips [17], and global invariant manifolds near a Shilnikov bifurcation in a laser model [2]. The interactions between Julia sets and stable/unstable manifolds are studied numerically in [42]. Dynamical transport and design of low energy transport in celestial mechanics, as discussed in [22, 33, 33, 47, 60, 72], is an outstanding example of the use of stable/unstable manifolds in applications. See also the work of [4, 5, 23, 24] on weak stability boundaries and geometric instability in Hamiltonian systems, as well the work of [68, 69] on spatial structure of galaxies.

Stable/unstable manifolds commonly appear in the geometric theory of dynamical systems as separatrices or transport barriers. We refer, for example, to the work of [55, 56, 57] on generalizations of Melnikov theory based on the study of stable/unstable manifolds and their intersections. Numerical methods for computing connecting orbits are often based on the idea

of solving a boundary value problem for orbits beginning on an unstable and terminating on a stable manifold. See, for example, the general numerical methods developed in [8, 26, 31] and also the lecture notes [25]. We also refer the interested reader to the works of [3, 62, 64] for discussion of numerical methods which combine high-order parameterization of the local stable/unstable manifolds with shooting methods for solving discrete time boundary value problems in order to compute connecting orbits for maps.

Of course, the references mentioned in this section barely scratch the surface of the relevant literature. The discussion above is only meant to provide some motivation and context for the present work within the existing literature.

3. A parameterization method for periodic orbits. Let $f\colon \mathbb{R}^M \to \mathbb{R}^M$ be a diffeomorphism, and recall that f^N denotes the composition of the map f with itself N times (let f^0 be the identity map). A period N point for the map f is a $p \in \mathbb{R}^M$, so that

$$f^N(p) = p;$$

i.e., p is a fixed point of the map f^N. We say that the point p is a hyperbolic period N point for f if p is a hyperbolic fixed point of f^N, i.e., if the matrix $Df^N(p)$ has no eigenvalues on the unit circle. We say that p has least period N if

$$f^j(p) \neq f^k(p) \quad \text{for } 1 \leq j \neq k \leq N.$$

In both numerical and theoretical considerations of period N points it is often useful to consider the following "multiple shooting" scheme. We introduce the variables $p = p_1$ and $f(p_j) = p_{j+1}$ for $j \geq 1$ and look for solutions of the following system of equations:

$$\begin{aligned} f(p_1) &= p_2 \\ f(p_2) &= p_3 \\ &\vdots \\ f(p_N) &= p_1. \end{aligned}$$

We refer to $p_1, \ldots, p_N$ as a periodic orbit for f. Motivated by this system of equations, we define also the mapping $F\colon \mathbb{R}^{M\times N} \to \mathbb{R}^{M\times N}$ by

$$F(p_1, \ldots, p_N) = \begin{pmatrix} f(p_N) \\ f(p_1) \\ \vdots \\ f(p_{N-1}) \end{pmatrix} \tag{13}$$

and note that if $(p_1, \ldots, p_N) \in \mathbb{R}^{M\times N}$ is a fixed point of F, then any of the points p_j, $1 \leq j \leq N$, is a period N point for f. Moreover if $p_i \neq p_j$ for $i \neq j$, then each of the p_j, $1 \leq j \leq N$, has least period N.

Note that the differential of F is given by

$$DF(p_1, \ldots, p_N) = \begin{pmatrix} 0 & 0 & \ldots & 0 & Df(p_N) \\ Df(p_1) & 0 & \ldots & 0 & 0 \\ 0 & Df(p_2) & \ldots & 0 & 0 \\ \vdots & \vdots & \ddots & \vdots & \vdots \\ 0 & 0 & \ldots & Df(p_{N-1}) & 0 \end{pmatrix}.$$

Moreover suppose that $\mathbf{p} = (p_1, \dots, p_N) \in \mathbb{R}^{M\times N}$ is a fixed point of F, and let $\lambda \in \mathbb{C}$ and $\xi = (\xi_1, \dots, \xi_N) \in \mathbb{R}^{M\times N}$. Then we have the following proposition.

Proposition 3.1. *Suppose that $\mathbf{p} \in \mathbb{R}^{MN}$ is a fixed point of F. Then λ, ξ is an eigenvalue/eigenvector pair for $DF(\mathbf{p})$ if and only if for each $1 \le j \le N$, $\sqrt[N]{\lambda}, \xi_j$ is an eigenvalue/eigenvector pair for $Df^N(p_j)$.*

Proof. Note that $\lambda \neq 0$, as f is a diffeomorphism. Moreover each of the matrices $Df(p_j)$ is invertible. Starting with $DF(\mathbf{p})\xi = \lambda\xi$ and rewriting it as the system

$$\begin{aligned} Df(p_N)\xi_N &= \lambda\xi_1 \\ Df(p_1)\xi_1 &= \lambda\xi_2 \\ &\vdots \\ Df(p_{N-1})\xi_{N-1} &= \lambda\xi_{N-1}, \end{aligned}$$

we get that

$$\begin{aligned} Df(p_{j+1})Df(p_j)\xi_j &= \lambda^2\xi_{j+2} \\ &\vdots \\ Df(p_{j-1})\cdots Df(p_1)Df(p_N)\cdots Df(p_j)\xi_j &= \lambda^N\xi_j, \end{aligned}$$

i.e., $Df^N(p_j)\xi_j = \lambda^N\xi_j$, by the chain rule. Reversing the computation gives the reverse implication. ∎

The proposition says that we recover the stability of each of the period N points p_j, $1 \le j \le N$, by computing the stability of the fixed point $\mathbf{p}$. Note that the proof also recovers the classic fact that if $p_1, \dots, p_N$ is a periodic orbit of least period N, then each of the periodic points has the same eigenvalues. Moreover the periodic orbit is hyperbolic if and only if $\mathbf{p}$ is a hyperbolic fixed point.

3.1. Composition-free invariance equations. Continuing the notation established in section 3, let $p_1, \dots, p_N \in \mathbb{R}^M$ be a hyperbolic periodic orbit of the smooth map $f\colon \mathbb{R}^M \to \mathbb{R}^M$, and let $\tilde{\lambda}_1, \dots, \tilde{\lambda}_m$ denote the stable eigenvalues of any of the matrices $Df^N(p_j)$, $1 \le j \le N$ (as each of these matrices has the same eigenvalues). Assume that each of the matrices $Df^N(p_j)$, $1 \le j \le N$, is diagonalizable, and let $\tilde{\xi}_1^{(j)}, \dots, \tilde{\xi}_m^{(j)}$ denote a linearly independent choice of eigenvectors. Motivated by the above considerations for periodic points, we develop a "multiple shooting" approach to the parameterization of stable/unstable manifolds for a period N point. Let

$$\lambda_j := \left(\tilde{\lambda}_j\right)^{\frac{1}{N}}$$

for each $1 \le j \le m$.

We look for smooth functions $P^{(j)}\colon B_1^m(0) \to \mathbb{R}^M$, $1 \le j \le N$, satisfying the first-order constraints

$$P^{(j)}(0) = p_j \quad \text{and} \quad \frac{\partial}{\partial\theta_k}P^{(j)}(0) = \xi_k^{(j)} \tag{14}$$

for $1 \le j \le N$ and $1 \le k \le m$, and solve the system of invariance equations

$$\begin{aligned} f\left(P^{(1)}\left(\theta_1,\ldots,\theta_m\right)\right) &= P^{(2)}\left(\lambda_1\theta_1,\ldots,\lambda_m\theta_m\right) \\ f\left(P^{(2)}\left(\theta_1,\ldots,\theta_m\right)\right) &= P^{(3)}\left(\lambda_1\theta_1,\ldots,\lambda_m\theta_m\right) \\ &\vdots \\ f\left(P^{(N-1)}\left(\theta_1,\ldots,\theta_m\right)\right) &= P^{(N)}\left(\lambda_1\theta_1,\ldots,\lambda_m\theta_m\right) \\ f\left(P^{(N)}\left(\theta_1,\ldots,\theta_m\right)\right) &= P^{(1)}\left(\lambda_1\theta_1,\ldots,\lambda_m\theta_m\right) \end{aligned} \tag{15}$$

for $\theta_1,\ldots,\theta_m \in B_1^m(0)$.

The following discussion explains our interest in this system. Suppose that $(P^{(1)},\ldots,P^{(N)}(\theta))$ is a solution of the system of (15). Then

$$f[P^{(1)}(\theta_1,\ldots,\theta_m)] = P^{(2)}(\lambda_1\theta_1,\ldots,\lambda_m\theta_m),$$

so that

$$f\left(f[P^{(1)}(\theta_1,\ldots,\theta_m)]\right) = f[P^{(2)}(\lambda_1\theta_1,\ldots,\lambda_m\theta_m)] = P^{(3)}(\lambda_1^2\theta_1,\ldots,\lambda_m^2\theta_m)$$

or

$$f^2[P^{(1)}(\theta_1,\ldots,\theta_m)] = P^{(3)}(\lambda_1^2\theta_1,\ldots,\lambda_m^2\theta_m).$$

Proceeding in this way leads to

$$f^k[P^{(1)}(\theta_1,\ldots,\theta_m)] = P^{(k+1)}(\lambda_1^k\theta_1,\ldots,\lambda_m^k\theta_m)$$

for $1 \le k \le N-1$, and finally

$$f^N[P^{(1)}(\theta_1,\ldots,\theta_m)] = P^{(1)}(\lambda_1^N\theta_1,\ldots,\lambda_m^N\theta_m),$$

which is

$$f^N[P^{(1)}(\theta_1,\ldots,\theta_m)] = P^{(1)}(\tilde{\lambda}_1\theta_1,\ldots,\tilde{\lambda}_m\theta_m),$$

so that $P^{(1)}$ satisfies the parameterization conjugacy equation for the composition map f^N. Repeating this computation for each $P^{(k)}$ with $2 \le k \le N$ gives the following.

Claim 3.2. If $P(\theta) := (P^1(\theta_1,\ldots,\theta_m),\ldots,P^{(N)}(\theta_1,\ldots,\theta_m))$ solves the system of equations given by (15), then $P^{(k)}$ parameterizes the local stable manifold at p_k for each $1 \le k \le N$.

To solve the system of invariance equations, we consider the case when f is analytic and look for formal series solutions

$$P^{(k)}(\theta_1,\ldots,\theta_m) = \sum_{|\alpha|=0}^{\infty} p_\alpha^{(k)}\theta^\alpha$$

or

$$P(\theta) = \sum_{|\alpha|=0}^{\infty} p_\alpha\theta^\alpha, \quad \text{where} \quad p_\alpha = \begin{pmatrix} p_\alpha^{(1)} \\ \vdots \\ p_\alpha^{(N)} \end{pmatrix}.$$

We will see that if $F\colon \mathbb{R}^{MN} \to \mathbb{R}^{MN}$ is the map defined in (13), and if $p = (p_1, \dots, p^N) \in \mathbb{R}^{MN}$ denotes the periodic orbit, then the coefficients of P solve homological equations of the form

$$[DF(p) - \lambda_1^{\alpha_1} \cdots \lambda_m^{\alpha_m} \mathrm{Id}_{\mathbb{R}^{MN}}]\, p_\alpha = S_\alpha. \tag{16}$$

Here S_α is a nonlinear function of the coefficients $\{p_\beta\}$ with $|\beta| < |\alpha|$, and the form of the nonlinearity of S_α depends only on the nonlinearity of f (rather than the nonlinearity f^N). Deriving the explicit form of S_α is a problem-dependent question best illustrated in specific examples.

Note that

$$\lambda_1^{\alpha_1} \cdots \lambda_m^{\alpha_m} = \lambda_k$$

for some $1 \le k \le N$ and some fixed multi-index $(\alpha_1, \dots, \alpha_m) \in \mathbb{Z}^m$ if and only if

$$\tilde{\lambda}_1^{\alpha_1} \cdots \tilde{\lambda}_m^{\alpha_m} = \tilde{\lambda}_k,$$

with the same data; i.e., the homological equations (16) have a unique solution p_α for each $\alpha \in \mathbb{N}^m$, $|\alpha| \ge 2$, if and only if the eigenvalues of $Df^N(p_k)$ are nonresonant. Then the "multiple-shooting" version of the parameterization method is applicable if and only if the standard version applies to the fixed point of the composition map.

Claim 3.3 (real analytic parameterizations). By appropriately choosing the eigenvectors, we can always arrange for the image of the parameterizations to be real.

Starting with a real eigenvalue and eigenvector of $Df^N(p_j)$, call it $u_1^{(j)}$, it is easy to see from the recursive equation $(Df^N(p_j) - \lambda^{Nn} I)u_\alpha^{(j)} = s_\alpha^{(j)}$ that $u_\alpha^{(j)}$ is real for all α. Now we rewrite $(DF(p_*) - \lambda^n I)u_\alpha = S_\alpha$ as a system using block multiplication, i.e.,

$$Df(p_N)u_\alpha^{(N)} - \lambda^\alpha u_\alpha^{(1)} = S_\alpha^{(1)}$$

and

$$Df(p_j)u_\alpha^{(j)} - \lambda^\alpha u_\alpha^{(j+1)} = S_\alpha^{(j+1)}$$

for $j = 1, \dots, N-1$. This system leads to

$$(Df(p_{j-1}) \cdots Df(p_1)Df(p_N) \cdots Df(p_j) - \lambda^{N\alpha} I)u_\alpha^{(j)} = \Sigma_\alpha^{(j)},$$

that is

$$(Df^N(p_j) - \lambda^{N\alpha} I)u_\alpha^{(j)} = \Sigma_\alpha^{(j)},$$

where

$$\begin{aligned}\Sigma_\alpha^{(j)} = {} & (Df(p_j) \cdots Df(p_1)Df(p_N) \cdots Df(p_{j+1}))S_\alpha^{(j)} \\ & + \lambda^\alpha (Df(p_j) \cdots Df(p_1)Df(p_N) \cdots Df(p_{j+2}))S_\alpha^{(j+1)} \\ & + \cdots \\ & + \lambda^{(N-1)\alpha} S_\alpha^{(j-1)}.\end{aligned}$$

Summarizing, we have that

$$\Sigma_\alpha^{(j)} = Df^N(p_{j+1})S_\alpha^{(j)} + \lambda^\alpha Df^{N-1}(p_{j+2})S_\alpha^{(j+1)} + \cdots + \lambda^{(N-1)\alpha}S_\alpha^{(j-1)}[*].$$

Now $(Df^N(p_j) - \lambda^{N\alpha}I)$ is a real matrix, and hence it is enough to ensure that $\Sigma_\alpha^{(j)}$ is real.

For $\Sigma_\alpha^{(j)}$, a finite sum of convolution terms, the above suggests to multiply $u_1^{(j-1)}$ by λ $\cdots$ and $u_1^{(j+1)}$ by λ^{N-1} . In practice, we multiply $u_1^{(j-1)}$ by a primitive N root of unity ρ $\cdots$ and multiply $u_1^{(j+1)}$ by ρ^{N-1}. Using automatic differentiation, the argument extends to non-polynomial nonlinearities as well.

For simplicity of the argument pick $u_1^{(N)}$ real; then using induction on $[*]$ we show that $u_\alpha^{(j)}\lambda^{N-j}$ is real for all α and j, and it also shows that multiplying $u_1^{(j)}$ by λ and recomputing $u_\alpha^{(j)}$ to evaluate $\hat{P}^{(j)}(\theta)$ is equivalent to computing $P^{(j)}(\lambda\theta)$.

Claim 3.4 (nonuniqueness and scaling the eigenvectors). By appropriately choosing the scalings of the eigenvectors, we can arrange that for Taylor series coefficients of the parameterizations to have whatever exponential decay rate we like.

To see this, note that Lemma 2.5 tells us that solutions of (4) are unique up to the choice of the scalings of the eigenvectors at the fixed point. The same follows for the system given by (15), precisely because solutions of the system of equations (15) are equivalent to solutions of (4) for the composition map.

Moreover we can work out exactly the effect of rescaling the eigenvectors on the Taylor coefficients of the solution. To this end, consider

$$P^{(k)}(\theta_1, \ldots, \theta_m) = \sum_{|\alpha|=0}^{\infty} p_\alpha^{(k)}\theta^\alpha$$

for $1 \le k \le m$ solving the system of equations (15), and suppose that the eigenvectors $\xi_j = (p_{e_j}^{(1)}, \ldots, p_{e_j}^{(N)})$ have $\|\xi_j\| = 1$. Now choose scalings $0 < \sigma_j$ for $1 \le j \le m$, and define the vector $\sigma = (\sigma_1, \ldots, \sigma_m)$, as well as the new collection of functions

$$\hat{P}^{(k)}(\theta_1, \ldots, \theta_m) = \sum_{|\alpha|=0}^{\infty} \hat{p}_\alpha^{(k)}\theta^\alpha,$$

where

$$\hat{p}_\alpha^{(k)} = \sigma^\alpha p_\alpha^{(k)}, \qquad 1 \le k \le m. \tag{17}$$

Note that

$$\hat{p}_0^{(k)} = \sigma^0 p_0^{(k)} = p_k$$

and

$$\hat{p}_{e_j}^{(k)} = \sigma^{e_j} p_0^{(k)} = \sigma_j p_{e_j}^{(k)};$$

i.e., $\hat{P}$ satisfies the first-order constraints given by (14).

Now define the new variables

$$\hat{\theta}_j = \frac{\theta_j}{\sigma_j}$$

for $1 \leq j \leq m$. Then

$$\begin{aligned}\hat{P}^{(k)}(\hat{\theta}_1, \ldots, \hat{\theta}_m) &= \sum_{|\alpha|=0}^{\infty} \hat{p}_\alpha^{(k)} \hat{\theta}^\alpha \\ &= \sum_{|\alpha|=0}^{\infty} \sigma^\alpha p_\alpha^{(k)} \hat{\theta}^\alpha \\ &= \sum_{|\alpha|=0}^{\infty} p_\alpha^{(k)} \theta^\alpha \\ &= P^{(k)}(\theta_1, \ldots, \theta_m),\end{aligned}$$

and

$$\begin{aligned}P^{(k)}(\lambda_1\theta_1, \ldots, \lambda_m\theta_m) &= f[P^{(k+1)}(\theta_1, \ldots, \theta_m)] \\ &= f[\hat{P}^{(k+1)}(\hat{\theta}_1, \ldots, \hat{\theta}_m)].\end{aligned}$$

Combining these observations gives that

$$f[\hat{P}^{(k+1)}(\hat{\theta}_1, \ldots, \hat{\theta}_m)] = \hat{P}^{(k)}(\lambda_1\hat{\theta}_1, \ldots, \lambda_m\hat{\theta}_m),$$

i.e., that $\hat{P}$ is the solution of the system given by (15), subject to the linear constraints with eigenvectors scaled by σ. By uniqueness, $\hat{P}$ is the only such solution. This shows that given one solution of (15) whose Taylor coefficients are $\{p_\alpha\}$, rescaling the eigenvectors by σ leads to a new solution of (15) whose Taylor coefficients are determined from $\{p_\alpha\}$ by (17).

3.2. Formal solution of the invariance equations. We now study the system of invariance equations (15) for a number of particular example problems. Our goal is to illustrate the derivation of the homological equations which are essential for numerically implementing the parameterization method.

3.2.1. A second worked out example: Stable/unstable manifolds of a period two orbit the for Hénon map using multiple shooting parameterization. In this section $f\colon \mathbb{R}^2 \to \mathbb{R}^2$ denotes the Hénon map defined in (7). Suppose that $p_0, q_0 \in \mathbb{R}^2$ is a saddle-type period two orbit for f, i.e., that

$$f(p_0) = q_0 \quad \text{and} \quad f(q_0) = p_0,$$

with $p_0 \neq q_0$, that there is $\tilde{\lambda} \in \mathbb{R}$ with $|\tilde{\lambda}| < 1$, and $\xi, \eta \in \mathbb{R}^2$ such that

$$Df^2(p_0)\xi = \tilde{\lambda}\xi \quad \text{and} \quad Df^2(q_0)\eta = \tilde{\lambda}\eta,$$

and that the remaining eigenvalue of $Df^2(p_0)$, $Df^2(q_0)$ is unstable. Define

$$\lambda = \sqrt{\tilde{\lambda}}.$$

In this setting the system of invariance equations given by (15) reduces to

$$\begin{aligned} f(Q(\theta)) &= P(\lambda\theta), \\ f(P(\theta)) &= Q(\lambda\theta). \end{aligned} \tag{18}$$

We look for P, Q of the form

$$P(\theta) = \sum_{n=0}^{\infty} p_n \theta^n$$

and

$$Q(\theta) = \sum_{n=0}^{\infty} q_n \theta^n$$

and require that

$$P(0) = p_0 \quad \text{and} \quad Q(0) = q_0$$

(so that q_0, p_0 denote the zeroth Taylor coefficient as well as the periodic orbit) and also that

$$P'(0) = p_1 = \xi \quad \text{and} \quad Q'(0) = q_1 = \eta,$$

so that P and Q are tangent to the correct eigenspaces.

We will derive the explicit form of the homological equation (16). To this end, note that

$$P(\lambda\theta) = \sum_{n=0}^{\infty} \lambda^n p_n \theta^n \quad \text{and} \quad Q(\lambda\theta) = \sum_{n=0}^{\infty} \lambda^n q_n \theta.$$

Writing

$$p_n = \begin{pmatrix} p_n^1 \\ p_n^2 \end{pmatrix} \quad \text{and} \quad q_n = \begin{pmatrix} q_n^1 \\ q_n^2 \end{pmatrix}$$

for the components of the Taylor coefficients, and employing the Cauchy product for power series, we have

$$f(P(\theta)) = \begin{pmatrix} 1 + \sum_{n=0}^{\infty} p_n^2 - \sum_{n=0}^{\infty} \sum_{k=0}^{n} a p_{n-k}^1 p_k^1 \\ \sum_{n=0}^{\infty} b p_n^1 \end{pmatrix}$$

and

$$f(Q(\theta)) = \begin{pmatrix} 1 + \sum_{n=0}^{\infty} q_n^2 - \sum_{n=0}^{\infty} \sum_{k=0}^{n} a q_{n-k}^1 q_k^1 \\ \sum_{n=0}^{\infty} b q_n^1 \end{pmatrix}.$$

Plugging these power series expansions into (18) and matching like powers of θ for $n \geq 2$ leads to

$$\begin{pmatrix} q_n^2 - \sum_{k=0}^{n} a q_{n-k}^1 q_k^1 \\ b q_n^1 \\ p_n^2 - \sum_{k=0}^{n} a p_{n-k}^1 p_k^1 \\ b p_n^1 \end{pmatrix} = \begin{pmatrix} \lambda^n p_n^1 \\ \lambda^n p_n^2 \\ \lambda^n q_n^1 \\ \lambda^n q_n^2 \end{pmatrix}$$

or

$$\begin{pmatrix} q_n^2 - 2a q_0^1 q_n^1 - \sum_{k=1}^{n-1} a q_{n-k}^1 q_k^1 \\ b q_n^1 \\ p_n^2 - 2a p_0^1 p_n^1 - \sum_{k=1}^{n-1} a p_{n-k}^1 p_k^1 \\ b p_n^1 \end{pmatrix} = \lambda^n \begin{pmatrix} p_n^1 \\ p_n^2 \\ q_n^1 \\ q_n^2 \end{pmatrix}.$$

We move terms of order n to the left, move terms of order less than n to the right, and observe that the dependence on p_n, q_n is linear. This results in the equations

$$\left[\begin{pmatrix} 0 & 0 & -2aq_0^1 & 1 \\ 0 & 0 & b & 0 \\ -2p_0^1 & 1 & 0 & 0 \\ b & 0 & 0 & 0 \end{pmatrix} - \lambda^n \begin{pmatrix} 1 & 0 & 0 & 0 \\ 0 & 1 & 0 & 0 \\ 0 & 0 & 1 & 0 \\ 0 & 0 & 0 & 1 \end{pmatrix} \right] \begin{bmatrix} p_n^1 \\ p_n^2 \\ q_n^1 \\ q_n^2 \end{bmatrix} = \begin{bmatrix} a \sum_{k=1}^{n-1} q_{n-k}^1 q_k^1 \\ 0 \\ a \sum_{k=1}^{n-1} p_{n-k}^1 p_k^1 \\ 0 \end{bmatrix}. \tag{19}$$

Letting $F\colon \mathbb{R}^4 \to \mathbb{R}^4$ be the map

$$F(p_1, p_2, q_1, q_2) = \begin{pmatrix} 1 + q_2 - a q_1^2 \\ b q_1 \\ 1 + p_2 - a p_1^2 \\ b p_1 \end{pmatrix},$$

we see that, indeed, (19) has exactly the form promised in (16). The point of working through the computation above is that we now know explicitly the form of the right-hand side of the homological equation, and this knowledge is used to implement numerical algorithms.

Note that for all $n \geq 2$, λ^n is not an eigenvalue of $DF(p_0, q_0)$. This is because we assumed that p_0, q_0 is a hyperbolic saddle, and hence the only other eigenvalue has absolute value greater than one. Then $|\lambda^n| < |\lambda| < 1$ for all $n \geq 2$, and hence λ^n is never an eigenvalue. Equation (19) is characteristic for $DF(p_0, q_0)$, and we have that solutions exist and are unique

for any right-hand side and $n \geq 2$. This is a specific instance of a more general result, namely that a saddle with exactly one stable eigenvalue is never resonant. Solving (19) recursively for each $2 \leq n \leq K$ leads to the polynomial approximations

$$P^K(\theta) = \sum_{n=0}^{K} p_n \theta^n \quad \text{and} \quad Q^K(\theta) = \sum_{n=0}^{K} q_n \theta^n.$$

Also note that if we consider instead the unstable eigenvalues, all of the comments above also apply to the case of unstable eigenvalues. We discuss numerical methods further in section 4.

3.2.2. The homological equations for a period N point of Henon. Suppose now that $p^1, \ldots, p^N \in \mathbb{R}^2$ is a periodic orbit of the Hénon map with least period N, and that $\tilde{\lambda} \in \mathbb{R}$ and $\xi^1, \ldots, \xi^N \in \mathbb{R}^2$ have that

$$Df^N(p^k)\xi^k = \tilde{\lambda}\xi^k$$

for $1 \leq k \leq N$. Define the map

$$F(x_1, y_1, x_2, y_2, \ldots, x_N, y_N) = \begin{pmatrix} 1 + y_N - a x_N^2 \\ b x_N \\ 1 + y_2 - a x_2^2 \\ b x_2 \\ \vdots \\ 1 + y_1 - a x_1^2 \\ b x_1 \end{pmatrix}.$$

Define

$$\lambda = \sqrt[N]{\tilde{\lambda}}.$$

Note that $p^1, \ldots, p^N$ is a fixed point of F and that $\tilde{\lambda}$, $\xi^1, \ldots, \xi^N$ can be computed by finding eigenvalues/eigenvectors for $DF(p^1, \ldots, p^N)$.

Let $p_0, p_1 \in \mathbb{R}^{2N}$ be

$$p_0 = \begin{pmatrix} p^1 \\ \vdots \\ p^N \end{pmatrix} \quad \text{and} \quad p_1 = \begin{pmatrix} \xi^1 \\ \vdots \\ \xi^N \end{pmatrix}.$$

We seek

$$P(\theta) = \begin{pmatrix} P^{(1)}(\theta) \\ \vdots \\ P^{(N)}(\theta) \end{pmatrix},$$

a solution to the invariance equation, with

$$P^{(k)}(\theta) = \sum_{n=0}^{\infty} p_n^k \theta^n$$

for $p_n^k \in \mathbb{R}^2$ for $1 \leq k \leq N$. We write $p_n^k = (p_{n,1}^k, p_{n,2}^k)$ to denote the components. Define $p_n \in \mathbb{R}^{2N}$ by

$$p_n = \begin{pmatrix} p_n^1 \\ \vdots \\ p_n^N \end{pmatrix}.$$

A computation similar to that illustrated in detail in section 3.2.1 shows that each $p_n \in \mathbb{R}^{2N}$ with $n \geq 2$ is a solution of the equation

$$[DF(p_0) - \lambda^n \mathrm{Id}_{2N\times 2N}]\, p_n = S_n^N,$$

with S_n^N defined by

$$S_n^N := \begin{pmatrix} a\sum_{k=1}^{n-1} p_{n-k,1}^N p_{k,1}^N \\ 0 \\ a\sum_{k=1}^{n-1} p_{n-k,1}^1 p_{k,1}^1 \\ 0 \\ \vdots \\ a\sum_{k=1}^{n-1} p_{n-k,1}^{N-1} p_{k,1}^{N-1} \\ 0 \end{pmatrix}.$$

Again, we see that the linear system has a unique solution for all $n \geq 2$ by the assumption that the orbit is hyperbolic, as $\lambda^n \neq \lambda$ for any $n \geq 2$. Solving the system to order K leads to the polynomial approximation

$$P_K(\theta) := \sum_{n=0}^{K} p_n \theta^n.$$

3.2.3. Example of a two-dimensional manifold for a three-dimensional map: Stable/unstable manifolds for periodic orbits of the Lomelí map. Consider the map $f\colon \mathbb{R}^3 \to \mathbb{R}^3$ given by

$$f(x,y,z) = \begin{pmatrix} z + Q(x,y) \\ x \\ y \end{pmatrix}, \tag{20}$$

where Q is the quadratic form

$$Q(x,y) = \alpha + \tau x + ax^2 + bxy + cy^2.$$

We refer to (20) as the Lomelí map. It is standard to choose parameters normalized so that $a + b + c = 1$. The Lomelí map is a normal form for quadratic volume-preserving maps with quadratic inverse. In that sense it can be thought of as a three-dimensional generalization of the planar Hénon map. The dynamics of the Lomelí map are considered in a number of studies; see, for example, [29, 53, 54, 62].

Now let

$$F(x_1, y_1, z_1, \ldots, x_N, y_N, z_N) = \begin{pmatrix} z_N + Q(x_N, y_N) \\ x_N \\ y_N \\ \vdots \\ z_1 + Q(x_1, y_1) \\ x_1 \\ y_1 \end{pmatrix}.$$

Suppose that $(p^1, \ldots, p^N) \in \mathbb{R}^{3N}$ is a fixed point of F; i.e., $p^1, \ldots, p^N$ is a periodic orbit.

We focus on the case which the orbit is hyperbolic with a complex conjugate pair of stable/unstable eigenvalues. More precisely, assume that $Df^N(p_k)$ has a complex conjugate pair of eigenvalues $\tilde{\lambda}, \bar{\tilde{\lambda}} \in \mathbb{C}$, and let $\xi^k, \bar{\xi}^k$ be an associated choice of complex conjugate eigenvectors. Take λ and $\bar{\lambda}$ complex conjugates with

$$\lambda = \sqrt[N]{\tilde{\lambda}} \quad \text{and} \quad \bar{\lambda} = \sqrt[N]{\bar{\tilde{\lambda}}}.$$

Of course we have again that $\lambda, \bar{\lambda}, \xi^1, \bar{\xi}^1, \ldots, \xi^N, \bar{\xi}^N$ can be found by computing eigenvalues/eigenvectors of $DF(p^1, \ldots, p^N)$.

In this case we employ complex variables and look for $P^{(k)} \colon \mathbb{C}^2 \to \mathbb{C}^3$ solving the invariance equations

$$\begin{aligned} f(P^{(N)}(z_1, z_2)) &= P^{(1)}(\lambda z_1, \bar{\lambda} z_2) \\ f(P^{(1)}(z_1, z_2)) &= P^{(2)}(\lambda z_1, \bar{\lambda} z_2) \\ &\vdots \\ f(P^{(N-1)}(z_1, z_2)) &= P^{(N)}(\lambda z_1, \bar{\lambda} z_2). \end{aligned}$$

We look for solutions in the form

$$P^{(k)}(z_1, z_2) = \sum_{n_1=0}^{\infty} \sum_{n_2=0}^{\infty} p^k_{n_1,n_2} z_1^{n_1} z_2^{n_2}$$

for each $1 \le k \le N$, where $p^k_{n_1,n_2} \in \mathbb{C}^3$ for each $n_1, n_2 \in \mathbb{N}$. The components are expressed as $p^k_{n_1,n_2} = (p^k_{n_1,n_2,1}, p^k_{n_1,n_2,2}, p^k_{n_1,n_2,3}) \in \mathbb{C}^3$. We write

$$p_0 = \begin{pmatrix} p^1 \\ \vdots \\ p^N \end{pmatrix}, \quad p_{1,0} = \begin{pmatrix} \xi^1 \\ \vdots \\ \xi^N \end{pmatrix}, \quad \text{and} \quad p_{0,1} = \begin{pmatrix} \bar{\xi}^1 \\ \vdots \\ \bar{\xi}^N \end{pmatrix},$$

for the zero- and first-order Taylor coefficients, and write more generally

$$P(z_1, z_2) = \sum_{n_1=0}^{\infty} \sum_{n_2=0}^{\infty} p_{n_1,n_2} z_1^{n_1} z_2^{n_2},$$

where

$$p_{n_1,n_2} = \begin{pmatrix} p^1_{n_1,n_2} \\ \vdots \\ p^N_{n_1,n_2} \end{pmatrix},$$

note that

$$P^{(k)}(\lambda z_1, \bar{\lambda} z_2) = \sum_{n_1=0}^{\infty} \sum_{n_2=0}^{\infty} \lambda^{n_1} \bar{\lambda}^{n_2} p^{(k)}_{n_1,n_2} z_1^{n_1} z_2^{n_2}$$

and (after using the two variable Cauchy product) that

$$f[P^{(k)}(z_1, z_2)] = \begin{pmatrix} \alpha + \sum_{n_1=0}^{\infty} \sum_{n_2=0} \infty \left(p^{(k)}_{n_1,n_2,3} + \tau p^{(k)}_{n_1,n_2,1} + q^{(k)}_{n_1,n_2} \right) z_1^{n_1} z_2^{n_2} \\ \sum_{n_1=0}^{\infty} \sum_{n_2=0}^{\infty} p^{(k)}_{n_1,n_2,1} \, z_1^{n_1} z_2^{n_2} \\ \sum_{n_1=0}^{\infty} \sum_{n_2=0}^{\infty} p^{(k)}_{n_1,n_2,2} \, z_1^{n_1} z_2^{n_2} \end{pmatrix},$$

where

$$q^{(k)}_{n_1,n_2} = \sum_{i=0}^{n_1} \sum_{j=0}^{n_2} a p^{(k)}_{n_1-i,n_2-j,1} p^{(k)}_{i,j,1} + b p^{(k)}_{n_1-i,n_2-j,1} p^{(k)}_{i,j,2} + c p^{(k)}_{n_1-i,n_2-j,2} p^{(k)}_{i,j,2}.$$

Matching like powers for $n_1 + n_2 \geq 2$ leads to

$$\begin{pmatrix} p^{(N)}_{n_1,n_2,3} + \tau p^{(N)}_{n_1,n_2,1} + q^{(N)}_{n_1,n_2} \\ p^{(N)}_{n_1,n_2,1} \\ p^{(N)}_{n_1,n_2,2} \end{pmatrix} = \lambda^{n_1} \bar{\lambda}^{n_2} \begin{pmatrix} p^{(1)}_{n_1,n_2,1} \\ p^{(1)}_{n_1,n_2,2} \\ p^{(1)}_{n_1,n_2,3} \end{pmatrix}$$

and

$$\begin{pmatrix} p^{(k-1)}_{n_1,n_2,3} + \tau p^{(k-1)}_{n_1,n_2,1} + q^{(k-1)}_{n_1,n_2} \\ p^{(k-1)}_{n_1,n_2,1} \\ p^{(k-1)}_{n_1,n_2,2} \end{pmatrix} = \lambda^{n_1} \bar{\lambda}^{n_2} \begin{pmatrix} p^{(k)}_{n_1,n_2,1} \\ p^{(k)}_{n_1,n_2,2} \\ p^{(k)}_{n_1,n_2,3} \end{pmatrix}$$

for $2 \leq k \leq N$. Let $s_{n_1,n_2} = (S^{(N)}_{n_1,n_2}, S^{(1)}_{n_1,n_2}, \ldots, S^{(N-1)}_{n_1,n_2})$ and

(21)

$$S^{(k)}_{n_1,n_2} = \begin{pmatrix} \sum_{i=0}^{n_1} \sum_{j=0}^{n_2} \delta^{n_1,n_2}_{j,k} \left(a p^{(k)}_{n_1-i,n_2-j,1} p^{(k)}_{i,j,1} + b p^{(k)}_{n_1-i,n_2-j,1} p^{(k)}_{i,j,2} + c p^{(k)}_{n_1-i,n_2-j,2} p^{(k)}_{i,j,2} \right) \\ 0 \\ 0 \end{pmatrix},$$

where we define

$$\delta_{j,k}^{n_1,n_2} := \begin{cases} 0 & \text{if } j = n_1 \text{ and } k = n_2, \\ 0 & \text{if } j = 0 \text{ and } k = 0, \\ 1 & \text{otherwise.} \end{cases}$$

Then

$$q_{n_1,n_2}^{(k)} = 2ap_{0,0,1}^{(k)} p_{n_1,n_2,1} + bp_{0,0,1} p_{n_1,n_2,2} + bp_{0,0,2} p_{n_1,n_2,1} + cp_{0,0,2} p_{n_1,n_2,2}.$$

Thus, the Taylor coefficient p_{n_1,n_2} is found by solving the homological equation

$$\left[DF(p_0) - \lambda^{n_1}\bar{\lambda}^{n_2}\mathrm{Id}_{3N\times 3N}\right] p_{n_1,n_2} = S_{n_1,n_2}. \tag{22}$$

Again we remark that these are always uniquely solvable in the case under consideration, namely a periodic hyperbolic saddle with a complex conjugate pair. This is because if $n_1+n_2 \geq 2$, then neither

$$\lambda^{n_1}\bar{\lambda}^{n_2} = \lambda \qquad \text{nor} \qquad \lambda^{n_1}\bar{\lambda}^{n_2} = \bar{\lambda}$$

is possible, and since the Lomelí map is volume-preserving, the third eigenvalue must have opposite stability from $\lambda, \bar{\lambda}$ (i.e., the eigenvalue is unstable if they are stable or vice versa). More generally a periodic orbit with a single complex conjugate pair of stable (or unstable) eigenvalues cannot be resonant.

We write

$$P_K(\theta) = \sum_{n=0}^{K} \sum_{m=0}^{n} p_{n-mm} \theta_1^{n-m} \theta_2^m$$

to denote the polynomial approximation obtained by solving the homological equations to order K.

Remark 3.5 (real parameterization). In the end, we are actually interested in the real dynamics of the Lomelí map and want the real image of P. By Considering (22), we see that solutions have the property

$$p_{m_2,m_1} = \overline{p_{m_1,m_2}}.$$

This complex conjugate property of the coefficients of P implies that if we choose complex conjugate variables

$$z_1 = \theta + i\phi \quad \text{and} \quad z_2 = \theta - i\phi$$

and define the polynomial

$$\hat{P}(\theta, \phi) = P(\theta + i\phi, \theta - i\phi),$$

where P has coefficients solving (22), then $\hat{P}$ parameterizes the real local stable/unstable manifolds associated with the periodic orbit.

3.2.4. Example of a nonpolynomial nonlinearity: Automatic differentiation for the standard map. We now consider the map $f\colon \mathbb{R}^2 \to \mathbb{R}^2$ given by

$$f(x,y) = \begin{pmatrix} x + a\sin(y) \\ y + x + a\sin(y) \end{pmatrix}, \tag{23}$$

with $a \geq 0$. The map is known as the *standard map*, or the Chirikov–Taylor map, and is widely studied as a toy model of symplectic dynamics [16, 36, 58]. For example, the mapping exhibits dynamics similar to the dynamics of a Poincaré section of a periodic orbit of a two freedom Hamiltonian system restricted to an energy surface. We now derive the homological equation for the parameterization of the stable/unstable manifold of a period N orbit of the standard map. This illustrates the use of our method for a system with nonpolynomial nonlinearities.

Then suppose that $p^1, \ldots, p^N \in \mathbb{R}^2$ are the points of a periodic orbit of least period N. Assume that the orbit is hyperbolic, and let $\xi^1, \ldots, \xi^N \in \mathbb{R}^2$ and $\tilde{\lambda} \in \mathbb{R}$ denote the associated eigenvalues and eigenvectors. We let

$$\lambda = \sqrt[N]{\tilde{\lambda}}$$

and look for solutions

$$P^{(k)}(\theta) = \sum_{n=0}^{\infty} p_n^{(k)} \theta^n$$

of (15) in this setting. Let us write

$$p_n^{(k)} = \begin{pmatrix} p_{n,1}^{(k)} \\ p_{n,2}^{(k)} \end{pmatrix}$$

for $1 \leq k \leq N$ to denote the components of $p_n^{(k)}$.

This difference between the present case and the examples discussed above is that the standard map has nonpolynomial nonlinearity, so that $f[P^{(k)}]$ cannot be evaluated directly using Cauchy products. Instead, we employ a technique sometimes called *automatic differentiation for Taylor series*, or simply automatic differentiation [46]. The idea is to exploit the fact that the sine and cosine functions are themselves solutions of simple differential equations.

Thus, define for each $1 \leq k \leq N$ the functions $S^{(k)}, C^{(k)}$ by

$$S^{(k)}(\theta) := \sin\left(P_2^{(k)}(\theta)\right)$$

and

$$C^{(k)}(\theta) := \cos\left(P_2^{(k)}(\theta)\right)$$

and look for the Taylor series expansions

$$\sum_{n=0}^{\infty} s_n^{(k)} \theta^n = S^{(k)}(\theta)$$

and

$$\sum_{n=0}^{\infty} c_n^{(k)} \theta^n = C^{(k)}(\theta).$$

Taking derivatives, we obtain

$$\frac{d}{d\theta} S^{(k)}(\theta) = \cos\left(P_2^{(k)}(\theta)\right) \frac{d}{d\theta} P_2^{(k)}(\theta)$$

and

$$\frac{d}{d\theta} C^{(k)}(\theta) = -\sin\left(P_2^{(k)}(\theta)\right) \frac{d}{d\theta} P_2^{(k)}(\theta),$$

which on the level of power series give

$$\begin{aligned}\sum_{n=0}^{\infty} (n+1) s_{n+1}^{(k)} \theta^n &= \left(\sum_{n=0}^{\infty} c_n \theta^n\right) \left(\sum_{n=0}^{\infty} (n+1) p_{n,2}^{(k)} \theta^n\right) \\ &= \sum_{n=0}^{\infty} \sum_{j=0}^{n} (j+1) c_{n-j}^{(k)} p_{j+1,2}^{(k)} \theta^n,\end{aligned}$$

and similarly

$$\sum_{n=0}^{\infty} (n+1) c_{n+1}^{(k)} \theta^n = -\sum_{n=0}^{\infty} \sum_{j=0}^{n} (j+1) s_{n-j}^{(k)} p_{j+1,2}^{(k)} \theta^n.$$

Of course we have

$$s_0^{(k)} = \sin\left(p_{0,2}^{(k)}\right) \quad \text{and} \quad c_0^{(k)} = \cos\left(p_{0,2}^{(k)}\right)$$

as well as

$$s_1^{(k)} = \cos\left(p_{0,2}^{(k)}\right) p_{1,2}^{(k)} \quad \text{and} \quad c_1^{(k)} = -\sin\left(p_{0,2}^{(k)}\right) p_{1,2}^{(k)}$$

Matching like powers of n for $n \geq 2$ give

$$s_n^{(k)} = \frac{1}{n} \sum_{j=1}^{n} j c_{n-j}^{(k)} p_{j,2}^{(k)} = c_0^{(k)} p_{n,2}^{(k)} + \frac{1}{n} \sum_{j=1}^{n-1} j c_{n-j}^{(k)} p_{j,2}^{(k)}$$

and

$$c_n^{(k)} = \frac{-1}{n} \sum_{j=1}^{n} j s_{n-j}^{(k)} p_{j,2}^{(k)} = -s_0^{(k)} p_{j,2}^{(k)} - \frac{1}{n} \sum_{j=1}^{n-1} j s_{n-j}^{(k)} p_{j,2}^{(k)}.$$

Now let

$$P(\theta) = \begin{pmatrix} P^{(1)}(\theta) \\ \vdots \\ P^{(N)}(\theta) \end{pmatrix}.$$

Then

$$P(\lambda\theta) = \sum_{n=0}^{\infty} \lambda^n p_n \theta^n,$$

while

$$\begin{aligned} f[P^{(k)}(\theta)] &= \begin{pmatrix} P_1^k(\theta) + a\sin\left(P_2^{(k)}(\theta)\right) \\ P_1^k(\theta) + P_2^{(k)}(\theta) + a\sin\left(P_2^{(k)}(\theta)\right) \end{pmatrix} \\ &= \sum_{n=0}^{\infty} \begin{pmatrix} p_{n,1}^{(k)} + as_n^{(k)} \\ p_{n,1}^{(k)} + p_{n,2}^{(k)} + as_n^{(k)} \end{pmatrix} \theta^n. \end{aligned}$$

The nth coefficient of this power series is

$$\begin{aligned} \begin{pmatrix} p_{n,1}^{(k)} + as_n^{(k)} \\ p_{n,1}^{(k)} + p_{n,2}^{(k)} + as_n^{(k)} \end{pmatrix} &= \begin{pmatrix} p_{n,1}^{(k)} + ac_0^{(k)} p_{n,2}^{(k)} + \dfrac{a}{n}\displaystyle\sum_{j=1}^{n-1} j c_{n-j}^{(k)} p_{j,2}^{(k)} \\ \\ p_{n,1}^{(k)} + p_{n,2}^{(k)} + ac_0^{(k)} p_{n,2}^{(k)} + \dfrac{a}{n}\displaystyle\sum_{j=1}^{n-1} j c_{n-j}^{(k)} p_{j,2}^{(k)} \end{pmatrix} \\ &= \begin{pmatrix} 1 & a\cos\left(p_{0,2}^{(k)}\right) \\ 1 & 1 + a\cos\left(p_{0,2}^{(k)}\right) \end{pmatrix} \begin{bmatrix} p_{n,1}^{(k)} \\ p_{n,2}^{(k)} \end{bmatrix} + \begin{bmatrix} \dfrac{a}{n}\displaystyle\sum_{j=1}^{n-1} j c_{n-j}^{(k)} p_{j,2}^{(k)} \\ \\ \dfrac{a}{n}\displaystyle\sum_{j=1}^{n-1} j c_{n-j}^{(k)} p_{j,2}^{(k)} \end{bmatrix}. \end{aligned}$$

Matching like powers in the invariance equations gives that the homological equation has the desired form

$$[DF(p_0) - \lambda^n \mathrm{Id}_{2N\times 2N}]\, p_n = \Sigma_n \tag{24}$$

for $n \geq 2$, where Σ_n is given by

$$\Sigma_n = \begin{pmatrix} \Sigma_n^{(N)} \\ \Sigma_n^{(1)} \\ \vdots \\ \Sigma_n^{(N-1)} \end{pmatrix}$$

and

$$\Sigma_n^{(k)} = \begin{pmatrix} \dfrac{-a}{n} \displaystyle\sum_{j=1}^{n-1} j c_{n-j}^{(k)} p_{n,2}^{(k)} \\ \dfrac{-a}{n} \displaystyle\sum_{j=1}^{n-1} j c_{n-j}^{(k)} p_{n,2}^{(k)} \end{pmatrix}$$

for $1 \le k \le N$.

Note that once $(p_{n,1}^{(k)}, p_{n,2}^{(k)})$ are computed as the components of the solution of the n-th homological equation (24), $s_{n+1}^{(k)}$ and $c_{n+1}^{(k)}$ are computed and stored for use in the solution of the $(n+1)$th homological equation. The automatic differentiation scheme just described allows us to compute the power series coefficients of the composition $\sin(P_2^{(k)}(\theta))$ for the cost of two Cauchy products. However, this approach requires us to store the coefficients $s_n^{(k)}$ and $c_n^{(k)}$ throughout the computation.

3.2.5. Further remarks on automatic differentiation: Nonlinearities given by the elementary functions of mathematical physics. The procedure discussed in section 3.2.4 can be made quite general. We elaborate briefly below, but the interested reader should also consult [11, 38, 45, 46, 74] for a more complete discussion. In particular, the first reference describes a general algorithmic framework for the manipulation of power series in nonlinear problems. The idea is that the *elementary functions of mathematical physics* comprising the nonlinear terms in many applied problems are themselves solutions of simple differential equations. This lets us extend the ideas exploited in section 3.2.4 to many other situations.

To formalize the discussion, suppose

$$P(\theta) = \sum_{n=0}^{\infty} p_n \theta^n, \qquad Q(\theta) = \sum_{n=0}^{\infty} q_n \theta^n, \qquad R(\theta) = \sum_{n=0}^{\infty} r_n \theta^n$$

are power series with $p_n, q_n, r_n \in \mathbb{C}$ for $n \ge 0$. The following lists several useful results for some common nonlinear functions.

- **Addition:** If $R(\theta) = P(\theta) + Q(\theta)$, then

$$r_n = p_n + q_n.$$

- **Multiplication:** If $R(\theta) = P(\theta)Q(\theta)$, then

$$r_n = \sum_{k=0}^{n} p_{n-k} q_k.$$

- **Division:** If $R(\theta) = P(\theta)/Q(\theta)$, then

$$r_n = \frac{1}{q_0} \left(p_n - \sum_{k=1}^{n} r_{n-k} q_k \right).$$

- **Powers:** If $\alpha \in \mathbb{C}$ and $R(\theta) = P(\theta)^\alpha$, then

$$r_n = \frac{1}{np_0} \sum_{k=0}^{n-1} (n\alpha - k(\alpha + 1))p_{n-k} r_k.$$

- **The natural exponential:** If $R(\theta) = e^{P(\theta)}$, then

$$r_n = \frac{1}{n} \sum_{k=0}^{n-1} (n-k) p_{n-k} r_k.$$

- **The natural logarithm:** If $R(\theta) = \log P(\theta)$, then

$$r_n = \frac{1}{p_0} \left(p_n - \frac{1}{n} \sum_{k=1}^{n-1} (n-k) r_{n-k} p_k \right).$$

- **Sine and cosine:** If $R(\theta) = \sin(P(\theta))$ and $Q(\theta) = \cos(P(\theta))$, then

$$r_n = \frac{-1}{n} \sum_{k=1}^{n} k q_{n-k} p_k$$

and

$$q_n = \frac{1}{n} \sum_{k=1}^{n} k r_{n-k} p_k.$$

See [45] for proofs. Using these formulas, one could apply the techniques of the present work to any map with nonlinearities given by the elementary functions. Moreover similar recursion can be obtained for other elementary functions such as Bessel functions, elliptic integrals, etc. Automatic differentiation techniques also extend to functions of several complex variables via the *radial gradient* method discussed in section 2.3.2 of [39].

4. Numerical implementation and example computations. The results of the previous section lead to numerical procedures as follows: for a period N orbit, find the m stable (or unstable) eigenvalues, and compute associated eigenvectors. This latter step involves an arbitrary choice of the scalings. Suppose that polynomial approximation to order $K \geq 2$ is desired and that the eigenvalues are nonresonant. Then solve the homological equations in increasing order 2, 3, ..., up to K. This leads to a collection of polynomials $P_K^1, \ldots, P_K^N \colon \mathbb{R}^m \to \mathbb{R}^M$.

The Kth order polynomials $P_K^j \colon \mathbb{R}^m \to \mathbb{R}^M$ for $1 \leq j \leq m$ are defined and analytic on all of $\mathbb{R}^m$. Of course we cannot expect the associated truncation error to be small on all $\mathbb{R}^m$, and we always restrict ourselves to a *numerical domain* on which the approximation is reasonable. Recall that by Claim 3.4 from section 3.1, we are free to fix the numerical domain as $B_1^m(0) \subset \mathbb{R}^m$ and choose the scalings of the eigenvectors so that the polynomial is well behaved on this domain. Evaluating the polynomials only for variables smaller than one leads to numerically stable results.

The only remaining question is how to choose the scalings of the eigenvectors. We would like to choose these scalings as large as possible so as to parameterize large regions of the stable/unstable manifold and hence learn as much as possible about the manifolds far from the periodic orbit. On the other hand, we also want the approximation to be reliable on $B_1^m(0)$. We quantify the notion of reliability by defining the *a posteriori error* associated with the polynomials $P_K^1, \dots, P_K^N$ as the positive number

$$\varepsilon_K := \max_{1\le j\le M} \left(\sup_{\theta\in B_1^m(0)} \left\| f(P_K^j(\theta_1,\dots,\theta_m)) - P_K^{j+1}(\lambda_1\theta_1,\dots,\lambda_m\theta_m) \right\| \right), \tag{25}$$

where we let $P_K^{N+1}(\theta) = P_K^1(\theta)$, i.e., impose periodicity. If the a posteriori error associated with P_K is small, this means that the conjugacy is approximately satisfied, and we are reasonable confident (but not certain) that our approximation is good.

The following describes an algorithm which, given an approximation order K and a desired numerical numerical tolerance ϵ_{tol}, adaptively rescales the eigenvectors until the scalings are as large as possible without exceeding the numerical tolerance. The discussion in the next section sheds further light on the procedure.

- **Inputs:** Choose a period N orbit and compute its eigenvectors scaled initially to length one. Fix a tolerance ϵ_{tol} and a polynomial order of approximation K.
- *Step* 1: Compute the Taylor coefficients of $P^1, \dots, P^N$ by solving the homological equations to order K.
- *Step* 2: Evaluate the a posteriori error ε_K defined in (25) (or as discussed in Remark 4.1 below).
- *Step* 3: If $\varepsilon_K < \epsilon_{\text{tol}}$, then the scale is increased and Step 2 is repeated. If $\epsilon_{\text{tol}} \le \varepsilon_K$, then the scale is decreased.
  Repeat steps 1 through 3 until ε_K is below but within (for example) 95% of ϵ_{tol}.

Remark 4.1 (analytic norms). In practice we can obtain efficient numerical bounds on the a posteriori error by computing only on the level of the coefficients. In fact if $g\colon \mathbb{C}^m \to \mathbb{C}$ is analytic on the unit poly-disk

$$D_1^m(0) := \left\{ z = (z_1,\dots,z_m) \in \mathbb{C}^m \mid \max_{1\le j\le m} |z_j| < 1 \right\},$$

then by the maximum modulus principle and the triangle inequality, we have

$$\sup_{\theta\in B_1^m(0)} |g(\theta)| \le \sup_{z\in \partial D_1^m(0)} |g(z)| \le \sum_{n=0}^{\infty} |g_n|,$$

where $g_n \in \mathbb{C}$ are the power series coefficients of g. Note that the inequality above holds even when one or more of the quantities are infinite. The final quantity on the right is an ℓ^1 norm on the Taylor coefficient, sometimes referred to as an analytic norm.

Consider the a posteriori error in (25) in the case that f is a polynomial. Then $f(P_K^j(\theta_1, \dots, \theta_m)$ and $P^{j+1}(\lambda_1\theta_1,\dots,\lambda_m\theta_m)$ are both polynomials so that

$$f(P_K^j(\theta_1,\dots,\theta_m)) - P_K^{j+1}(\lambda_1\theta_1,\dots,\lambda_m\theta_m) = \sum_{|\alpha|=0}^{\hat{K}} e_\alpha \theta^\alpha$$

for some $e_\alpha \in \mathbb{R}^M$. Moreover the coefficients e_α are computed at the cost of an evaluation of f (on a polynomial). Then we can bound the a posteriori error by

$$\varepsilon_K \leq \sum_{|\alpha|=0}^{\hat{K}} \|e_\alpha\|.$$

If $P_K^1,\dots,P_K^N$ are good approximations, then the coefficients e_α will be small, and this provides a good bound. If f is not a polynomial, then we must include a Taylor remainder bound in the estimates above.

4.1. A detailed numerical example: Eigenvector scalings and the size of the local manifold embedding. Returning to the Hénon map as defined in (7), consider the classic parameter values of $a = 1.4$ and $b = 0.3$, and note that the points

$$p_0 = \begin{pmatrix} -0.475800051175056 \\ 0.292740015352517 \end{pmatrix} \quad \text{and} \quad q_0 = \begin{pmatrix} 0.975800051175056 \\ -0.142740015352517 \end{pmatrix}$$

have $f(p_0) = q_0$ and $f(q_0) = p_0$; i.e., they provide a period two orbit. We check that $Df^2(p_0)$ has an unstable eigenvalue of $\tilde{\lambda} = -3.010100667740269$ (of course this is also an unstable eigenvalue of $Df^2(q_0)$) and choose associated eigenvectors

$$\tilde{\xi} = \begin{pmatrix} 0.807903584327622 \\ -0.097548838689916 \end{pmatrix} \quad \text{and} \quad \tilde{\eta} = \begin{pmatrix} -0.564145799517692 \\ -0.139698029289516 \end{pmatrix}.$$

Taking $\lambda = \sqrt{\tilde{\lambda}} = 1.734964169007611i$, we have the necessary ingredients to solve the homological equations (19) and compute polynomial charts $P(\theta)$ and $Q(\theta)$ for the local unstable manifolds of the period two orbit to any desired finite order of approximation K.

Suppose (somewhat arbitrarily) that, given the choice of eigenvectors above, we compute the parameterizations to order $K = 50$. We evaluate the resulting polynomials P^K and Q^K on the unit domain $\theta \in [-1, 1]$ and obtain the approximations illustrated in the left frame of Figure 4. Now we make several remarks.

- The simultaneous computation of the 51 two-dimensional Taylor coefficients $p_0,\dots,p_{50}$, $q_0,\dots,q_{50} \in \mathbb{C}^2$ of P^K and Q^K (i.e., solution of the homological equations to order K) takes 0.004 seconds using MATLAB on a Mac Pro with a 3.7 GHz quad-core Intel Xenon E5 processor. (All the computation times discussed in the paper are attached to this desktop.)
- Checking the conjugacy for each of the two manifolds at 500 uniformly spaced sample points in $[-1, 1]$ yields an a posteriori error estimate of $\epsilon = 1.33 \times 10^{-15}$.
- The image of P^K (blue curve in the left frame of Figure 4) has arc length

$$\int_{-1}^{1} \sqrt{\left(\frac{d}{d\theta}P_1^K(\theta)\right)^2 + \left(\frac{d}{d\theta}P_2^K(\theta)\right)^2}\, d\theta \approx 1.4.$$

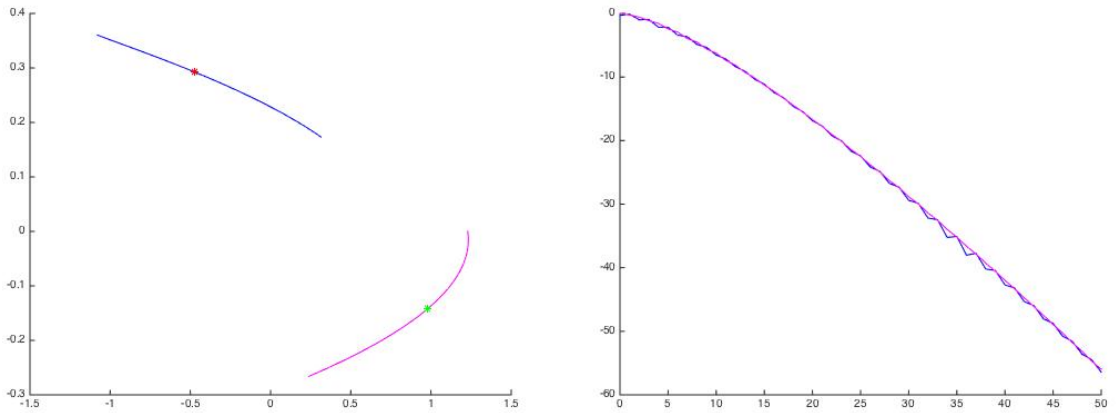

Figure 4. *Parameterized unstable manifold of a period two orbit of the Hénon map: polynomial approximation to order $K = 50$ using an eigenvector of unit length. The resulting error is on the order of 10^{-15}. Left: the top-left (blue) curve is the manifold attached to p_0, and the bottom-right (magenta) curve is the manifold attached to q_0. Each curve is the image of the unit interval, and each has arc length approximately 1.4. Right: base 10 logarithm of the Taylor coefficients as a function of order. Each Taylor coefficient is a vector with two components, and we plot only the log of the norm. Colors in the right frame match the conventions in the left frame. Coefficient computation takes 0.004 seconds.*

Note that since the parameterizations are given by polynomials, the arc length integrals can be evaluated almost exactly using a power series method. Only computing the square root of a power series—using the powers law is a reference to a formula in section 3.2.5 with $\alpha = 1/2$—requires truncation. The arc length for Q^K (magenta curve in the left frame of Figure 4) is also approximately 1.4.

- The logarithm base 10 of the magnitude of the Taylor coefficients is plotted versus the order of the coefficient in the right frame of Figure 4. The coefficients decay exponentially fast, and the coefficients of order 50 have magnitude 10^{-60}.

A closer look at the right frame of Figure 4 suggests that the coefficients of the parameterization are decaying too fast to be numerically significant after an order of about $K = 25$, (For $n \geq 25$, the magnitude of the Taylor coefficients of both polynomials is below 10^{-16}, i.e., below double precision machine epsilon). It is therefore reasonable to rescale the eigenvector to get a slower decay rate. Keeping the same numerical domain of $[-1, 1]$, we should expect the result to parameterize a larger section of the local unstable manifold.

Running the computations a second time, keeping $K = 50$, and taking

$$p_1 = 10\tilde{\xi} \quad \text{and} \quad q_1 = 10\tilde{\eta}$$

results in the parameterizations illustrated in Figure 5. Again, the computation takes 0.004 seconds and results in a conjugacy error on the order of $\epsilon = 10^{-7}$. However, the arc length of the manifolds is now about 7.3. The resulting local unstable manifold parameterizations suggest a substantial portion of the Hénon attractor, as seen in the left frame of Figure 5. Note that in this example the Taylor coefficients initially grow, reaching a maximum length of almost 10^4 before the exponential decay kicks in. The order $N = 50$ coefficients have magnitude approximately 10^{-7}, which is roughly the magnitude of the conjugacy error.

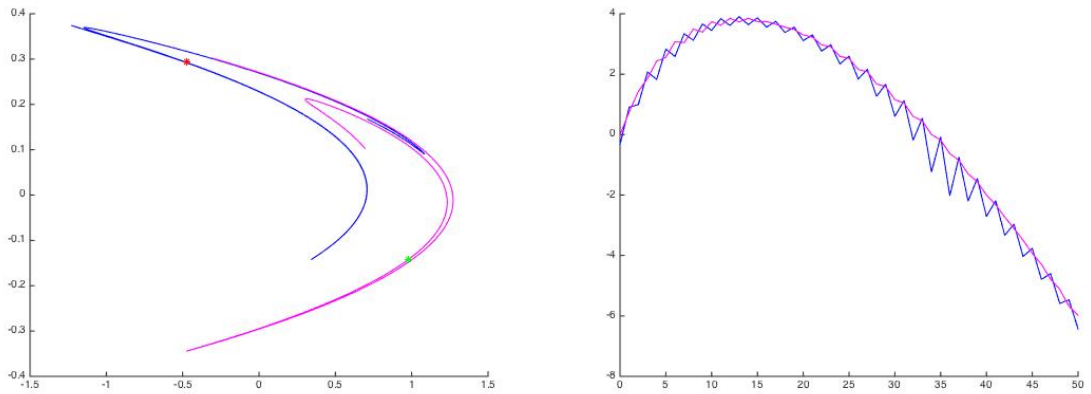

Figure 5. *Rescaled local parameterizations: polynomial approximation to order* $K = 50$ *using an eigenvector of length* 10. *The resulting error is on the order of* 10^{-7}. *New curves have arc length approximately* 7.3. *Color conventions are as in Figure* 4. *Coefficient computation takes* 0.004 *seconds.*

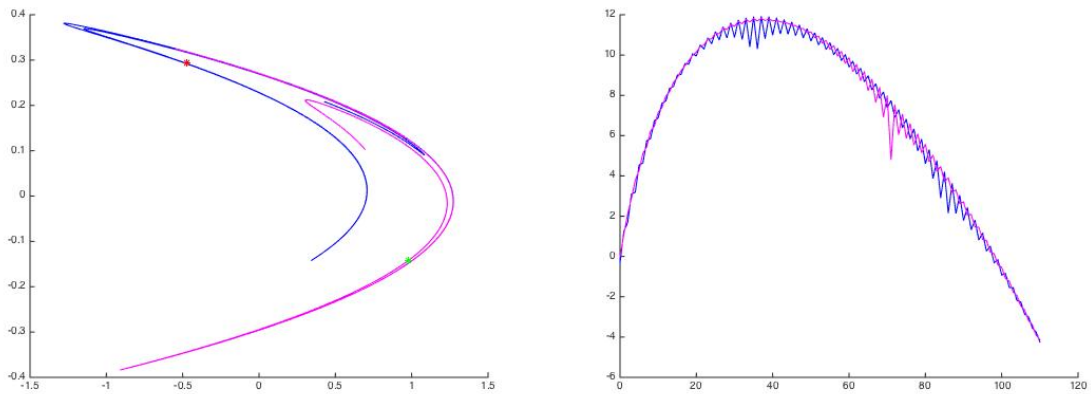

Figure 6. *Rescaled local parameterizations: polynomial approximation to order* $N = 110$ *using an eigenvector of length* 22. *The resulting error is on the order of* 10^{-4}. *New curves have arc length approximately* 12.1. *Color conventions are as in Figure* 4. *Coefficient computation takes* 0.0085 *seconds.*

Indeed, if we keep this scaling factor of 10 but compute the manifolds to order $N = 60$, then the resulting manifolds have the same length and look exactly like the parameterizations illustrated in the left frame of Figure 5. But the $N = 60$ coefficient is on the order of 10^{-12} in magnitude, and the resulting conjugacy error is on the order of 10^{-12}.

We remark that while increasing the order of the computation past $N = 60$ does lead to smaller coefficients, it does not further improve the conjugacy error. But it is easy to see why. Note that the largest polynomial coefficient is on the order of 10^4, so that the smallest numerically significant coefficients are those of order 10^{-12} (a 16-digit spread). To obtain more accurate results we would have to use extended precision computations.

Figure 6 illustrates a final result, which seems to be near the limit of what can be done in this example using only double precision arithmetic. The local parameterizations are

computed to polynomial order $N = 110$, with the initial eigenvectors scaled by a factor of 22. Each curve has arc length roughly 12.1, and the computation takes roughly 0.0085 seconds. The Conjugacy error is $\epsilon = 6.9 \times 10^{-4}$, and the resulting local manifold parameterizations uncover even more of the Hénon attractor. However, increasing the eigenvector scaling further results in polynomial approximations which diverge visibly.

Remark 4.2 (numerical implementation). The interested reader can reproduce these results by running the program

```
henonPer2Ex1_paper.m
```

which is available for free download from the authors' webpage for the preprint version of this paper [34]. By changing only the variables `N` and `scale`, one obtains any of the results above. The interested reader is invited to experiment with these computations.

4.2. Comparison with the naive approach. The computational advantages of the multiple-shooting parameterization method developed in the present work are seen clearly when we repeat the computation of section 4.1 using the naive approach. More precisely, we compute the parameterization of the local unstable manifold associated with the fixed point p_0 of the composition map $f \circ f = g$, where g is as given in (8).

Taking the approximation order $K = 60$ and iteratively solving the homological equation developed in section 2.3 results in a polynomial approximation that we denote by R^N. We compare this with our earlier results for the same manifold, already reported in Figure 5. Carefully choosing the scaling of the eigenvector in the computation of R^N (scaling it to 6.512 where the eigenvector in the computation of P^N was scaled to 8) provides the results illustrated in Figure 7. The Figure makes clear the virtue of the carefully chosen scaling: we obtain almost exactly the same local parameterization of the unstable manifold that we had before ("same" in the sense of both the embedding in phase space and the Taylor coefficient decay). That there exists such a choice of scaling is not a surprise: the two methods compute the same manifold.

However, the Naive computation takes about 0.035 seconds—or almost a factor of five times as long as the computation using the multiple shooting approach—after which we obtain only one of the two manifolds computed in section 4.1. Computing both manifolds takes 10 times as long as the multiple shooting approach. In addition, the conjugacy error is an order of magnitude worse than the multiple shooting case.

The poorer run time results from the need to compute the triple and quadruple Cauchy products appearing in the composition map (composition of the quadratic Hénon map with itself). Indeed, a more telling comparison between the two methods is to count floating point operations in the evaluation of the right-hand sides of the respective homological equations. Recalling (19), we see that the right-hand side of the homological equation for the multiple-shooting method requires evaluation of only two quadratic Cauchy products, while by (12), the right-hand side of the homological equation for the composition approach requires two quadratic Cauchy products as well as a cubic and a quartic evaluation. For the computations illustrated in Figure 7, evaluating the right-hand side of the homological equations in the

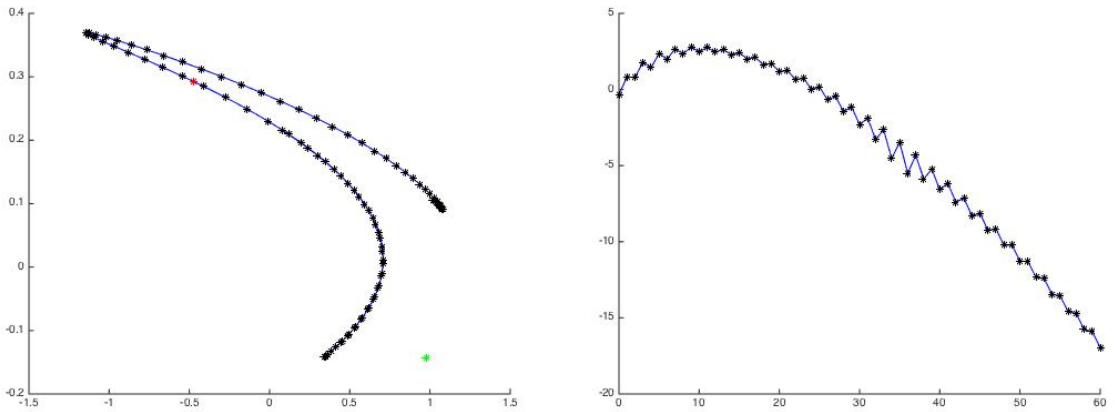

Figure 7. *Composition versus multiple shooting: unstable manifold of p_0 computed two ways. Blue curve corresponds to the parameterization computed using multiple shooting. Computational parameters are the same as reported in Figure 5. The black stars illustrate the same manifold, computed as the unstable manifold of a fixed point of the composition map. The results look identical, but the composition approach takes five times as long to compute and requires more than 300 times as many floating point operations. The error using the composition approach is more than an order of magnitude worse.*

naive approach is more than 300 times as expensive to compute than the right-hand side for the multiple-shooting parameterization method.

The interested reader can repeat these computations by running the program

`henonPer2_withComp.m`.

We remark that on many laptop and desktop computers (less powerful than the Mac Pro) the multiple-shooting method over performs the naive method by an even greater factor than reported above.

4.3. Long periodic orbits for the Hénon map. One strength or our algorithm is that it applies to periods much higher than two. Figure 8 illustrates the results of our procedure applied to a single orbit of period $M = 95$ for the Henon map with the classic parameters $a = 1.4$ and $b = 0.3$. The 2×95 parameterization functions are approximated to polynomial order $M = 50$, and we employ the adaptive rescaling algorithm with a desired tolerance of $\epsilon_{\text{tol}} = 10^{-14}$. The algorithm results in an eigenvector scaling of $s = 5.37$ for the stable and $s = 2.74$ for the unstable manifold.

Remark 4.3 (finding orbits of long period). We find periodic orbits (long or otherwise) for the Hénon map as follows. We pick any point "near" the attractor (say $x = 0$, $y = 1$) and iterate a large number of times (say $K = 10^5$ or more). Ignoring the first, say 100, points on the resulting orbit segment, we have a collection of points near the attractor. We now search this collection for orbits which are approximately period M for every $2 \leq M \leq M_{\max}$. For the Hénon map, we typically take $M_{\max} < 100$.

When we find an orbit segment which is approximately period M, we run a Newton method to obtain a better orbit. We also check that the orbit we obtain has not already been

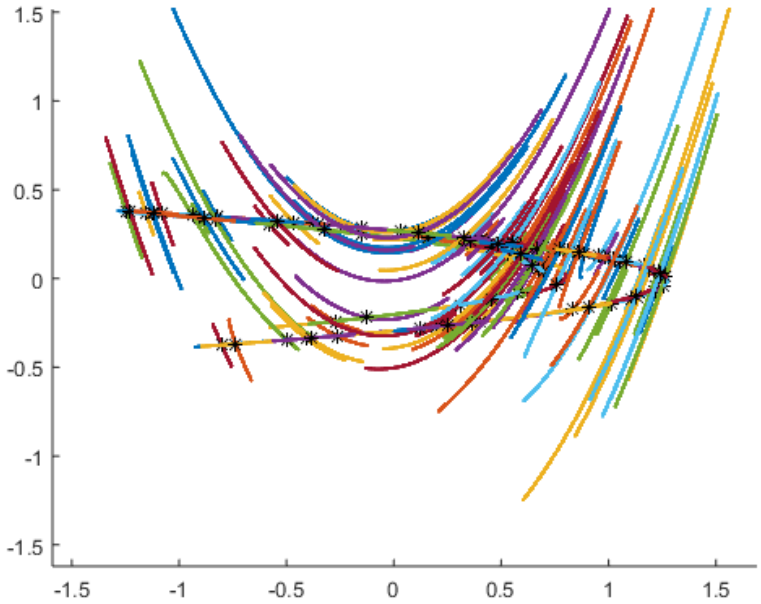

Figure 8. *Manifolds attached to a period* 95 *orbit for the Hénon map: classic parameter values, approximation order* $N = 50$*, and eigenvectors with optimal scaling. A posteriori error held below* 10^{-14}*. Unstable manifolds are tangent to the attractors, and stable manifolds are normal. Colors are chosen at random.*

found. If the orbit is new, that is, if M is the least period of the orbit, then we add it to our list. This is a typical search procedure based on the notion that the dynamics on the attractor are uniquely ergodic; hence a single long orbit should convey the same information as sampling "uniformly" over the attractor. The procedure just described was also used to find the orbits discussed in Remark 1.2 and illustrated in Figure 1.

4.4. Long periodic orbits in the standard map. In this section we consider several example results for the standard map given by (23) with $a = 2.1$, i.e., far from the integrable/perturbative case. Recall that this map has transcendental nonlinearity given by the sine function. Once we choose a periodic orbit of period M, we compute the Taylor coefficients by solving the homological equations given by (24). For example, the top frame of Figure 9 illustrates the local unstable manifolds attached to a period four point approximated to polynomial order $N = 200$. The eigenvector is scaled to $s = 1.6$.

The bottom frame of Figure 9 illustrates the stable/unstable manifolds attached to a period 25 orbit of the standard map, again approximated to polynomial order $N = 200$. The stable and unstable manifolds are scaled by $s = 0.95$ and $s = 0.98$, respectively. The inlay in the figure "zooms in" on one of the quasi-periodic islands (or secondary tori) surrounding the primary family of invariant circles in the standard map. This island shows yet another layer of islands (or tertiary tori), and our period 25 orbit is the hyperbolic "twin" of the (presumed) period 25 elliptic orbit in the center of the tertiary tori. The local stable/unstable manifolds parameterized here already show homoclinic intersections.

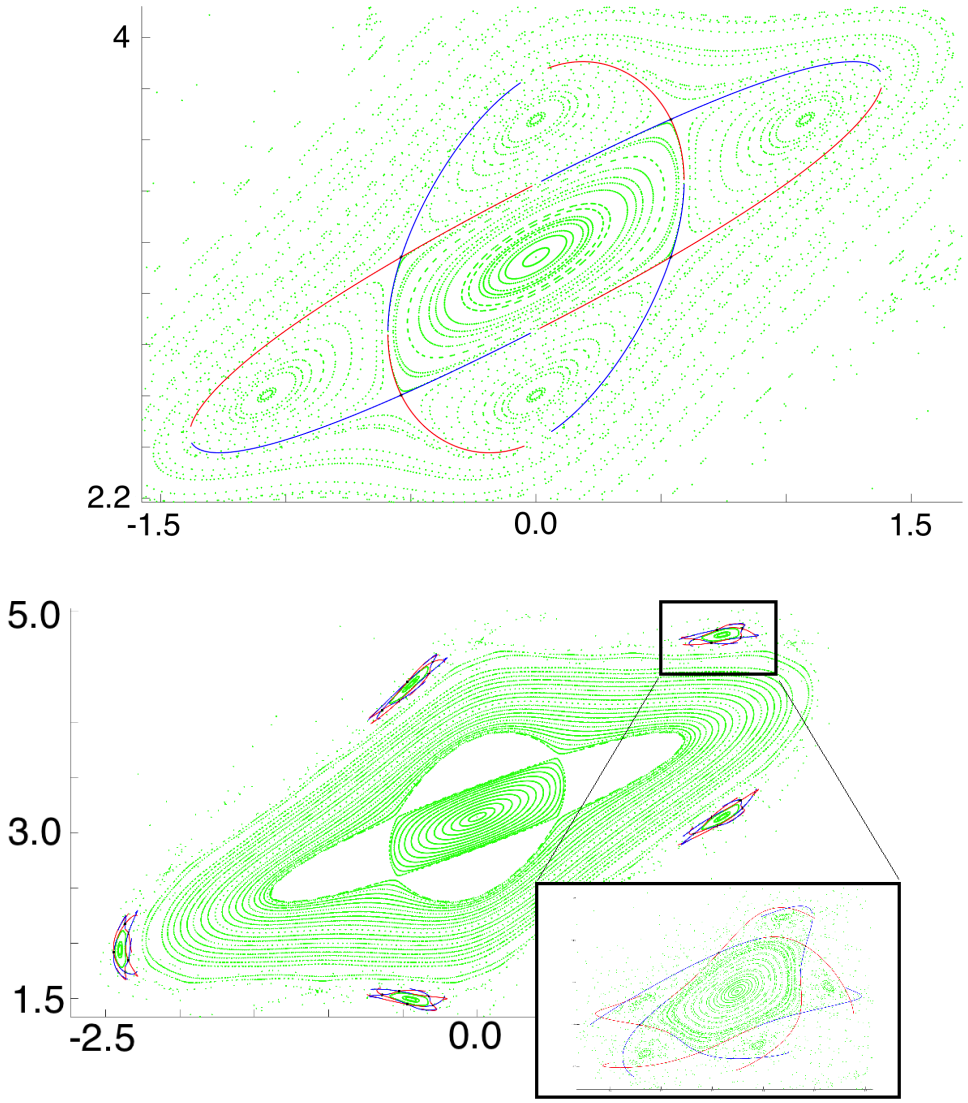

Figure 9. *The standard map with $a = 2.1$: elliptic island near the fixed point at $(0, \pi)$. The green points illustrate the dynamics of "typical orbits" and are obtained by simply iterating a large number of sample points. Viewing the hyperbolic dynamics requires a more deliberate approach. Top: local stable and unstable manifolds attached to a period four orbit. Bottom: local stable and unstable manifolds attached to a period 25 orbit. Inlay zooms in around a secondary torus and illustrates homoclinic intersection points. Unstable manifolds are blue and stable manifolds are red.*

The interested reader can repeat these computations by running the programs

`standardMapPaperEx_per4.m`

and

`standardMapPaperEx_per25.m`.

Remark 4.4 (finding long periodic orbits for the standard map). The standard map is an area preserving map, and hence it has no nontrivial attractor. The full map is not uniquely ergodic, and the strategy described in Remark 4.3 will not work. Moreover, simply sampling the phase space can be misleading, as there are many invariant circles which will be hard to distinguish from long periodic orbits numerically.

The orbits in the examples above are found by "eyeballing" the phase space portrait and looking for interesting features. For example, looking only at the green points in Figure 9, we see that the dominant feature is the period four KAM islands around the primary family of circles about the origin.

Standard results for area-preserving maps tell us to expect an elliptic period four orbit in the middle of these islands, and also that the elliptic period four point should have an associated twin, that is, there should be a hyperbolic period four orbit nearby. A simple inspection of the picture suggests that one point near this orbit is $x = -0.5$, $y = 2.5$. We run a Newton method with this as the initial condition and obtain the hyperbolic period four point accurate to machine precision. Computing the eigenvectors and solving the homological equations is straightforward. The initial guess for the period 25 orbit was obtained in precisely the same manner.

4.5. Period four vortex bubble in the Lomelí map. From the planar examples mentioned in the previous sections, one can learn a great deal about the dynamics of the system simply by phase space sampling. For example, iterating almost any initial point in the plane for long enough under the Hénon map yields the familiar picture of the attractor. Similarly, the green points in Figures 9 give a reasonable impression of the dynamics in the standard map for $a = 2.1$.

For dissipative maps of $\mathbb{R}^3$, things are not so different. Such maps typically have attractors, and simply iterating a collection of points provides a good picture of the dynamics. For volume-preserving maps of $\mathbb{R}^3$, the situation is somewhat less clear.

Consider, for example, the Lomelí map given by (20). Plotting a typical bounded orbit of the system leads to an amorphous blob. And plotting many such orbits results in a "thick" point cloud that may tell us very little. The system, however, does admit many invariant tori.

Figure 10, for example, illustrates a number of orbits for the system with parameters $a = 0.5$, $b = -0.5$, $c = 1$, $\tau = 1.333333333$, and $\alpha = 0.3444444444$. These orbits illustrate some period four invariant tori, secondary period four tori (or invariant circles?) about these, and finally a single invariant torus enclosing the entire structure. For each object, we are simply iterating a single point, which is presumably near the invariant torus or circle, and we do not have a parameterization of the tori.

Moreover these orbits are not "typical": rather, they were identified by eye as "interesting" results from a rather larger sampling of phase space. Such a search is both time consuming and ad hoc. Nevertheless it yields some interesting period four structure. The reader interested in the dynamics of the Lomelí map may want to review the works of [15, 29, 53, 54, 62, 64]. Indeed, the period four tori discussed here are also seen in [54].

The strategy of simply iterating points and examining the results for structure will not directly tell us anything about hyperbolic objects. However, based on these results we can

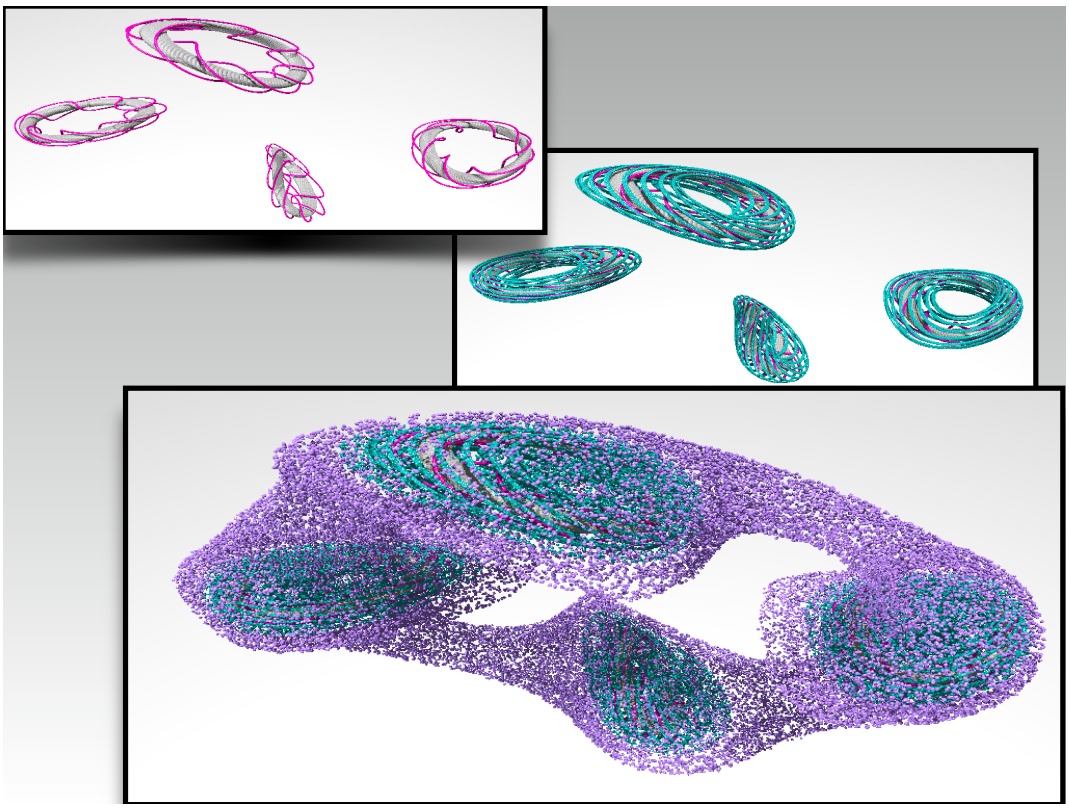

Figure 10. *Quasi-periodic invariant objects for the Lomelí map: Top left: period four invariant tori encircled by invariant circles. Middle right: same tori with longer invariant circles. Bottom: period one invariant torus encasing the period four structure. All of these invariant structures were located by phase space sampling.*

guess that there should be a pair of hyperbolic period four points near the top and bottom of the opening of the period four torus. Similarly, we can guess (or work out directly by hand) that there are a pair of fixed points near the top and bottom of the opening of the larger surrounding torus.

Once we have located the period four points (or fixed points), it is a simple procedure to compute the corresponding eigenvectors and solve the homological equations for the one- and two-dimensional stable/unstable manifolds attached to them. The results are illustrated in Figure 11. These parameterized local manifolds, when combined with the quasi-periodic structures found through phase space sampling, provide substantial insight into the phase space structure of the system.

The interested reader can repeat these computations by running the program

`lomeliPerMScript2D.m.`

We remark that the computations for the two-dimensional manifolds have not been optimized for speed, but the computations run in less than a minute.

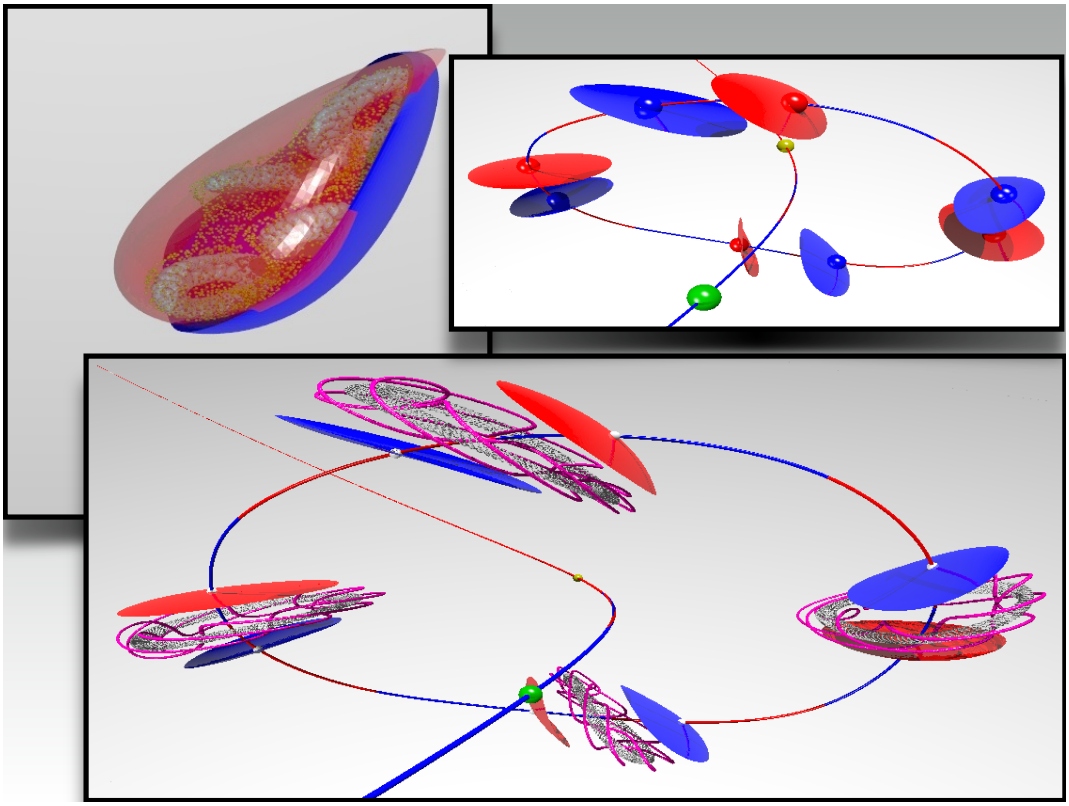

Figure 11. *Hyperbolic invariant objects for the Lomelí map: Top left:* $2d$ *local stable/unstable manifolds of the fixed points. Quasi-periodic invariant tori (periods one and four) seen inside. Top right:* $1d$ *stable/unstable manifolds attached to the fixed points (green and yellow spheres). Also shown are* $1d$ *and* $2d$ *stable/unstable manifolds attached to the period four points. Bottom: the stable/unstable manifolds of fixed points and period four orbit along with the period four invariant tori.*

5. Conclusions.

This work presents a framework for efficient and automatic high-order computation of polynomial approximations of local stable/unstable manifolds attached to periodic orbits of maps. We gave example computations illustrating the application of our method to long periodic orbits (up to period 100 or more) to maps with nonpolynomial nonlinearities, and to manifolds of dimensions one and two (though in principle our techniques apply to manifolds of any dimension). Several features of the method are that it recovers the dynamics on the manifold, that it can follow folds in the embedding, and that it admits a natural notion of a posteriori error.

We also compared the multiple-shooting parameterization method with a naive application of the parameterization method for fixed points of the composition map. Here we see clearly that while both methods accurately compute the local manifolds, the multiple-shooting approach is much more efficient in terms of runtime, floating point operations, and accuracy. Moreover, from the point of view of implementation, a major advantage of the multiple-shooting approach is that, regardless of the period of the orbit, we deal only with the nonlinearity of the original map. If, on the other hand, we compute compositions, we face exponential growth of the complexity of the nonlinearity.

In practice the high-order parameterizations developed here are often "global enough" to uncover homoclinic connections. This suggests that the method could be helpful in computer-assisted existence proofs, a topic which will be the object of future study. Indeed, it seems possible to combine the techniques of [32] with the recent work of [20, 43] and the parameterization method of the present study to obtain computer-assisted proofs of homoclinic and heteroclinic connecting dynamics for infinite-dimensional systems. Another interesting project would be to apply the methods of the present work to the difficult stable/unstable manifold computations of the period five point discussed in [7]. Unfortunately, the explicit form of the map used for that study is not given in the reference (however, the authors remark that the map is an 11th-order polynomial, a fact which suggests that the multiple-shooting approach of the present work could be a great help).

Another interesting direction of future research would be to apply rigorous globalization methods such as those of [66, 78] to grow the local manifolds studied here. This could lead to a better understanding of the connecting orbit structure and topological entropy for discrete time systems.

Acknowledgments. The authors would like to thank the three anonymous referees who read the submitted version of the manuscript for making a number of helpful suggestions. The final version is much improved thanks to their efforts.

REFERENCES

[1] P. Aguirre, E. J. Doedel, B. Krauskopf, and H. M. Osinga, *Investigating the consequences of global bifurcations for two-dimensional invariant manifolds of vector fields*, Discrete Contin. Dyn. Syst. Ser. A, 29 (2011), pp. 1309–1344, https://doi.org/10.3934/dcds.2011.29.1309.

[2] P. Aguirre, B. Krauskopf, and H. M. Osinga, *Global invariant manifolds near a Shilnikov homoclinic bifurcation*, J. Comput. Dyn., 1 (2014), pp. 1–38, https://doi.org/10.3934/jcd.2014.1.1.

[3] S. Anastassiu, T. Bountis, and A. Bäcker, *Homoclinic Points of 2-d and 4-d Maps via the Parameterization Method*, preprint, arXiv:1605.05521, 2016.

[4] E. Belbruno, M. Gidea, and F. Topputo, *Weak stability boundary and invariant manifolds*, SIAM J. Appl. Dyn. Syst., 9 (2010), pp. 1061–1089, https://doi.org/10.1137/090780638.

[5] E. Belbruno, M. Gidea, and F. Topputo, *Geometry of weak stability boundaries*, Qual. Theory Dyn. Syst., 12 (2013), pp. 53–66, https://doi.org/10.1007/s12346-012-0069-x.

[6] M. Berz, S. Newhouse, and A. Wittig, *Computer assisted proofs of the existence of high-period fixed points*, in Proceedings of the Fields Institute, http://bt.pa.msu.edu/cgi-bin/display.pl?name=FPTM08.

[7] M. Berz and A. Wittig, *High period fixed points, stable and unstable manifolds, and chaos in accelerator transfer maps*, Vestnik S.-Petersburg Univ., 10 (2014), pp. 93–110.

[8] W.-J. Beyn, *The numerical computation of connecting orbits in dynamical systems*, IMA J. Numer. Anal., 10 (1990), pp. 379–405, https://doi.org/10.1093/imanum/10.3.379.

[9] W.-J. Beyn and W. Kless, *Numerical Taylor expansions of invariant manifolds in large dynamical systems*, Numer. Math., 80 (1998), pp. 1–38, https://doi.org/10.1007/s002110050357.

[10] M. Breden, J. Lessard, and J. Mireles James, *Computation of maximal local (un)stable manifold patches by the parameterization method*, Indag. Math., 27 (2016), pp. 340–367.

[11] M. Bücker, G. Corliss, U. Naumann, P. Hovland, and B. Norris, eds., *Automatic Differentiation: Applications, Theory, and Implementations*, Lecture Notes in Comput. Sci. Eng. 50, Springer-Verlag, Berlin, 2006, https://doi.org/10.1007/3-540-28438-9.

[12] X. Cabré, E. Fontich, and R. de la Llave, *The parameterization method for invariant manifolds. I. Manifolds associated to non-resonant subspaces*, Indiana Univ. Math. J., 52 (2003), pp. 283–328.

[13] X. Cabré, E. Fontich, and R. de la Llave, *The parameterization method for invariant manifolds. II. Regularity with respect to parameters*, Indiana Univ. Math. J., 52 (2003), pp. 329–360.
[14] X. Cabré, E. Fontich, and R. de la Llave, *The parameterization method for invariant manifolds. III. Overview and applications*, J. Differential Equations, 218 (2005), pp. 444–515.
[15] M. J. Capiński and J. D. Mireles James, *Validated computation of heteroclinic sets*, SIAM J. Appl. Dyn. Syst., 16 (2017), pp. 375–409, https://doi.org/10.1137/16M1060674.
[16] B. V. Chirikov, *A universal instability of many-dimensional oscillator systems*, Phys. Rep., 52 (1979), pp. 263–379, https://doi.org/10.1016/0370-1573(79)90023-1.
[17] J. L. Creaser, B. Krauskopf, and H. M. Osinga, *α-flips and T-points in the Lorenz system*, Nonlinearity, 28 (2015), pp. R39–R65, https://doi.org/10.1088/0951-7715/28/3/R39.
[18] S. Day, R. Frongillo, and R. Treviño, *Algorithms for rigorous entropy bounds and symbolic dynamics*, SIAM J. Appl. Dyn. Syst., 7 (2008), pp. 1477–1506, https://doi.org/10.1137/070688080.
[19] S. Day and W. D. Kalies, *Rigorous computation of the global dynamics of integrodifference equations with smooth nonlinearities*, SIAM J. Numer. Anal., 51 (2013), pp. 2957–2983, https://doi.org/10.1137/120903129.
[20] R. de la Llave and J. Mireles James, *Parameterization of invariant manifolds by reducibility for volume preserving and symplectic maps*, Discrete Contin. Dyn. Syst. Ser. A, 32 (2012), pp. 4321–4360, https://doi.org/10.3934/dcds.2012.32.4321.
[21] M. Dellnitz and A. Hohmann, *A subdivision algorithm for the computation of unstable manifolds and global attractors*, Numer. Math., 75 (1997), pp. 293–317, https://doi.org/10.1007/s002110050240.
[22] M. Dellnitz, O. Junge, W. S. Koon, F. Lekien, M. W. Lo, J. E. Marsden, K. Padberg, R. Preis, S. D. Ross, and B. Thiere, *Transport in dynamical astronomy and multibody problems*, Internat. J. Bifur. Chaos Appl. Sci. Engrg., 15 (2005), pp. 699–727, https://doi.org/10.1142/S0218127405012545.
[23] A. Delshams, M. Gidea, R. de la Llave, and T. M. Seara, *Geometric approaches to the problem of instability in Hamiltonian systems. An informal presentation*, in Hamiltonian Dynamical Systems and Applications, NATO Sci. Peace Secur. Ser. B Phys. Biophys., Springer, Dordrecht, 2008, pp. 285–336, https://doi.org/10.1007/978-1-4020-6964-2_13.
[24] A. Delshams, M. Gidea, and P. Roldán, *Transition map and shadowing lemma for normally hyperbolic invariant manifolds*, Discrete Contin. Dyn. Syst., 33 (2013), pp. 1089–1112.
[25] E. J. Doedel, *Lecture notes on numerical analysis of bifurcation problems*, in International Course on Bifurcations and Stability in Structural Engineering, Université Pierre et Marie Curie (Paris VI), 2000.
[26] E. J. Doedel and M. J. Friedman, *Numerical computation of heteroclinic orbits*, J. Comput. Appl. Math., 26 (1989), pp. 155–170, https://doi.org/10.1016/0377-0427(89)90153-2.
[27] E. J. Doedel, B. Krauskopf, and H. M. Osinga, *Global invariant manifolds in the transition to preturbulence in the Lorenz system*, Indag. Math. (N.S.), 22 (2011), pp. 222–240, https://doi.org/10.1016/j.indag.2011.10.007.
[28] A. Douady and J. H. Hubbard, *Étude dynamique des polynômes complexes*, Pub. Math. d'Orsay 84, Université de Paris-Sud, Dép. de Mathématique, Orsay, France, 1984.
[29] H. R. Dullin and J. D. Meiss, *Quadratic volume-preserving maps: Invariant circles and bifurcations*, SIAM J. Appl. Dyn. Syst., 8 (2009), pp. 76–128, https://doi.org/10.1137/080728160.
[30] V. Franceschini and L. Russo, *Stable and unstable manifolds of the Hénon mapping*, J. Statist. Phys., 25 (1981), pp. 757–769, https://doi.org/10.1007/BF01022365.
[31] M. J. Friedman and E. J. Doedel, *Numerical computation and continuation of invariant manifolds connecting fixed points*, SIAM J. Numer. Anal., 28 (1991), pp. 789–808, https://doi.org/10.1137/0728042.
[32] Z. Galias and P. Zgliczyński, *Infinite-dimensional Krawczyk operator for finding periodic orbits of discrete dynamical systems*, Internat. J. Bifur. Chaos Appl. Sci. Engrg., 17 (2007), pp. 4261–4272, https://doi.org/10.1142/S0218127407019937.
[33] G. Gómez, W. S. Koon, M. W. Lo, J. E. Marsden, J. Masdemont, and S. D. Ross, *Connecting orbits and invariant manifolds in the spatial restricted three-body problem*, Nonlinearity, 17 (2004), pp. 1571–1606, https://doi.org/10.1088/0951-7715/17/5/002.
[34] J. Gonzalez and J. D. Mireles James, *High-Order Parameterization of Stable/Unstable Manifolds for Long Periodic Orbits of Maps*, preprint, 2017, http://cosweb1.fau.edu/~jmirelesjames/periodicParmManifoldPage.html.

[35] R. H. Goodman and J. K. Wróbel, *High-order bisection method for computing invariant manifolds of two-dimensional maps*, Internat. J. Bifur. Chaos Appl. Sci. Engrg., 21 (2011), pp. 2017–2042, https://doi.org/10.1142/S0218127411029604.

[36] J. M. Greene, R. S. MacKay, F. Vivaldi, and M. J. Feigenbaum, *Universal behaviour in families of area-preserving maps*, Phys. D, 3 (1981), pp. 468–486, https://doi.org/10.1016/0167-2789(81)90034-8.

[37] J. Guckenheimer and A. Vladimirsky, *A fast method for approximating invariant manifolds*, SIAM J. Appl. Dyn. Syst., 3 (2004), pp. 232–260, https://doi.org/10.1137/030600179.

[38] A. Haro, *Automatic Differentiation Methods in Computational Dynamical Systems: Invariant Manifolds and Normal Forms of Vector Fields at Fixed Points*, manuscript.

[39] A. Haro, M. Canadell, J.-L. Figueras, A. Luque, and J. M. Mondelo, *The Parameterization Method for Invariant Manifolds: From Rigorous Results to Effective Computations*, Appl. Math. Sci. 195, Springer, Cham, 2016, https://doi.org/10.1007/978-3-319-29662-3.

[40] M. E. Henderson, *Computing invariant manifolds by integrating fat trajectories*, SIAM J. Appl. Dyn. Syst., 4 (2005), pp. 832–882, https://doi.org/10.1137/040602894.

[41] M. Hénon, *A two-dimensional mapping with a strange attractor*, Comm. Math. Phys., 50 (1976), pp. 69–77.

[42] S. Hittmeyer, B. Krauskopf, and H. M. Osinga, *Interactions of the Julia set with critical and (un)stable sets in an angle-doubling map on* $\mathbb{C}\backslash\{0\}$, Internat. J. Bifur. Chaos Appl. Sci. Engrg., 25 (2015), 1530013, https://doi.org/10.1142/S021812741530013X.

[43] J. D. M. James, *Fourier–Taylor approximation of unstable manifolds for compact maps: Numerical implementation and computer assisted error bounds*, Found. Comput. Math., 2016, pp. 1–57 https://doi.org/10.1-007/s10208-016-9325-9.

[44] T. Johnson and W. Tucker, *A note on the convergence of parametrised nonresonant invariant manifolds*, Qual. Theory Dyn. Syst., 10 (2011), pp. 107–121, https://doi.org/10.1007/s12346-011-0040-2.

[45] À. Jorba and M. Zou, *A software package for the numerical integration of ODEs by means of high-order Taylor methods*, Experiment. Math., 14 (2005), pp. 99–117, http://projecteuclid.org/getRecord?id=euclid.em/1120145574.

[46] D. E. Knuth, *The Art of Computer Programming. Vol. 2: Seminumerical Algorithms*, 2nd ed., Addison-Wesley Ser. Comput. Sci. Inform. Process., Addison-Wesley, Reading, MA, 1981.

[47] W. S. Koon, M. W. Lo, J. E. Marsden, and S. D. Ross, *Low energy transfer to the moon*, Celestial Mech. Dyn. Astronom., 81 (2001), pp. 63–73, https://doi.org/10.1023/A:1013359120468.

[48] B. Krauskopf and H. Osinga, *Globalizing two-dimensional unstable manifolds of maps*, Internat. J. Bifur. Chaos Appl. Sci. Engrg., 8 (1998), pp. 483–503, https://doi.org/10.1142/S0218127498000310.

[49] B. Krauskopf and H. Osinga, *Growing* $1D$ *and quasi-*$2D$ *unstable manifolds of maps*, J. Comput. Phys., 146 (1998), pp. 404–419, https://doi.org/10.1006/jcph.1998.6059.

[50] B. Krauskopf and H. M. Osinga, *Computing geodesic level sets on global (un)stable manifolds of vector fields*, SIAM J. Appl. Dyn. Syst., 2 (2003), pp. 546–569, https://doi.org/10.1137/030600180.

[51] B. Krauskopf and H. M. Osinga, *The Lorenz manifold as a collection of geodesic level sets*, Nonlinearity, 17 (2004), pp. C1–C6, https://doi.org/10.1088/0951-7715/17/1/000.

[52] B. Krauskopf, H. M. Osinga, E. J. Doedel, M. E. Henderson, J. Guckenheimer, A. Vladimirsky, M. Dellnitz, and O. Junge, *A survey of methods for computing (un)stable manifolds of vector fields*, Internat. J. Bifur. Chaos Appl. Sci. Engrg., 15 (2005), pp. 763–791, https://doi.org/10.1142/S0218127405012533.

[53] H. E. Lomelí, J. D. Meiss, and K. E. Lenz, *Quadratic volume preserving maps: An extension of a result of Moser*, Regul. Chaotic Dyn., 3 (1998), pp. 122–131, https://doi.org/10.1070/rd1998v003n03ABEH000085.

[54] H. E. Lomelí and J. D. Meiss, *Quadratic volume-preserving maps*, Nonlinearity, 11 (1998), pp. 557–574, https://doi.org/10.1088/0951-7715/11/3/009.

[55] H. E. Lomelí and J. D. Meiss, *Heteroclinic intersections between invariant circles of volume-preserving maps*, Nonlinearity, 16 (2003), pp. 1573–1595, https://doi.org/10.1088/0951-7715/16/5/302.

[56] H. E. Lomelí and J. D. Meiss, *Resonance zones and lobe volumes for exact volume-preserving maps*, Nonlinearity, 22 (2009), pp. 1761–1789, https://doi.org/10.1088/0951-7715/22/8/001.

[57] H. E. Lomelí, J. D. Meiss, and R. Ramírez-Ros, *Canonical Melnikov theory for diffeomorphisms*, Nonlinearity, 21 (2008), pp. 485–508, https://doi.org/10.1088/0951-7715/21/3/007.

[58] R. S. MacKay, *A renormalisation approach to invariant circles in area-preserving maps*, Phys. D, 7 (1983), pp. 283–300, https://doi.org/10.1016/0167-2789(83)90131-8.
[59] K. Makino and M. Berz, *Taylor models and other validated functional inclusion methods*, Int. J. Pure Appl. Math., 4 (2003), pp. 379–456.
[60] J. J. Masdemont, *High-order expansions of invariant manifolds of libration point orbits with applications to mission design*, Dyn. Syst., 20 (2005), pp. 59–113, https://doi.org/10.1080/14689360412331304291.
[61] J. Mireles James, *Polynomial approximation of one parameter families of (un)stable manifolds with rigorous computer assisted error bounds*, Indag. Math., 26 (2015), pp. 225–265.
[62] J. D. Mireles James, *Quadratic volume-preserving maps: (Un)stable manifolds, hyperbolic dynamics, and vortex-bubble bifurcations*, J. Nonlinear Sci., 23 (2013), pp. 585–615.
[63] J. D. Mireles James, *Computer assisted error bounds for linear approximation of (un)stable manifolds and rigorous validation of higher dimensional transverse connecting orbits*, Comm. Nonlinear Sci. Numer. Simul., 22 (2015), pp. 1102–1133.
[64] J. D. Mireles James and H. Lomelí, *Computation of heteroclinic arcs with application to the volume preserving Hénon family*, SIAM J. Appl. Dyn. Syst., 9 (2010), pp. 919–953, https://doi.org/10.1137/090776329.
[65] J. D. Mireles James and K. Mischaikow, *Rigorous a posteriori computation of (un)stable manifolds and connecting orbits for analytic maps*, SIAM J. Appl. Dyn. Syst., 12 (2013), pp. 957–1006, https://doi.org/10.1137/12088224X.
[66] S. Newhouse, M. Berz, J. Grote, and K. Makino, *On the estimation of topological entropy on surfaces*, in Geometric and Probabilistic Structures in Dynamics, Contemp. Math. 469, AMS Providence, RI, 2008, pp. 243–270, https://doi.org/10.1090/conm/469/09170.
[67] C. Robinson, *Dynamical systems: Stability, Symbolic Dynamics, and Chaos*, Stud. Adv. Math., CRC Press, Boca Raton, FL, 1998.
[68] M. Romero-Gómez, E. Athanassoula, J. J. Masdemont, and C. García-Gómez, *Invariant manifolds as building blocks for the formation of spiral arms and rings in barred galaxies*, in Chaos in Astronomy, Astrophys. Space Sci. Proc., Springer, Berlin, 2009, pp. 85–92.
[69] M. Romero-Gómez, P. Sánchez-Martín, and J. J. Masdemont, *How invariant manifolds form spirals and rings in barred galaxies*, Butl. Soc. Catalana Mat., 29 (2014), pp. 51–75.
[70] C. Simo, *On the analytical and numerical approximation of invariant manifolds*, in Modern Methods in Celestial Mechanics, Ecole de Printemps d'Astrophysique de Goutelas (France), D. Benest, and C. Froeschle, eds., Gif-sur-Yvette: Editions Frontieres, 1990, pp. 285–329.
[71] S. Smale, *Differentiable dynamical systems*, Bull. Amer. Math. Soc., 73 (1967), pp. 747–817.
[72] M. Tantardini, E. Fantino, Y. Ren, P. Pergola, G. Gómez, and J. J. Masdemont, *Spacecraft trajectories to the L_3 point of the Sun–Earth three-body problem*, Celestial Mech. Dynam. Astronom., 108 (2010), pp. 215–232, https://doi.org/10.1007/s10569-010-9299-x.
[73] W. Tucker, *A rigorous ODE solver and Smale's 14th problem*, Found. Comput. Math., 2 (2002), pp. 53–117, http://dx.doi.org/10.1007/s002080010018.
[74] W. Tucker, *Validated Numerics: A Short Introduction to Rigorous Computations*, Princeton University Press, Princeton, NJ, 2011.
[75] W. Tucker and D. Wilczak, *A rigorous lower bound for the stability regions of the quadratic map*, Phys. D, 238 (2009), pp. 1923–1936, https://doi.org/10.1016/j.physd.2009.06.020.
[76] J. B. van den Berg, J. D. Mireles James, and C. Reinhardt, *Computing (un)stable manifolds with validated error bounds: Non-resonant and resonant spectra*, J. Nonlinear Sci., 26 (2016), pp. 1055–1095, https://doi.org/10.1007/s00332-016-9298-5.
[77] D. Wilczak, *Uniformly hyperbolic attractor of the Smale–Williams type for a Poincaré map in the Kuznetsov system*, SIAM J. Appl. Dyn. Syst., 9 (2010), pp. 1263–1283, https://doi.org/10.1137/100795176.
[78] A. Wittig, M. Berz, J. Grote, K. Makino, and S. Newhouse, *Rigorous and accurate enclosure of invariant manifolds on surfaces*, Regul. Chaotic Dyn., 15 (2010), pp. 107–126, https://doi.org/10.1134/S1560354710020024.
[79] J. K. Wróbel and R. H. Goodman, *High-order adaptive method for computing two-dimensional invariant manifolds of three-dimensional maps*, Commun. Nonlinear Sci. Numer. Simul., 18 (2013), pp. 1734–1745, https://doi.org/10.1016/j.cnsns.2012.10.017.